Advances in Nano Research, *Vol. 15, No. 2 (2023) 113-128*
https://doi.org/10.12989/anr.2023.15.2.113

Buckling and bending of coated FG graphene-reinforced composite plates and shells

Ahmed Amine Daikh[1,2], Amin Hamdi[3], Hani M. Ahmed[3], Mohamed S. Abdelwahed[4]
Alaa A. Abdelrahman[5] and Mohamed A. Eltaher*[4,5]

[1]*Department of Technology, University Centre of Naama, 45000, Algeria*
[2]*Laboratoire d'Etude des Structures et de Mécanique des Matériaux, Département de Génie Civil, Faculté des Sciences et de la Technologie, Université Mustapha Stambouli, Mascara, Algerie*
[3]*Department of Civil and Environmental Engineering, Faculty of Engineering, King Abdulaziz University, Jeddah, Saudi Arabia*
[4]*Mechanical Engineering Department, Faculty of Engineering, King Abdulaziz University, P.O. Box 80204, Jeddah, Saudi Arabia*
[5]*Mechanical Design & Production Department, Faculty of Engineering, Zagazig University, Zagazig 44519, Egypt*

(*Received September 15, 2021, Revised March 2, 2023, Accepted May 16, 2023*)

Abstract. The advancement of theoretical research has numerous challenges, particularly with regard to the modeling of structures, in contrast to experimental investigation of the mechanical behavior of complex systems. The main objective of this investigation is to provide an analytical analysis of the static problem of a new generation of composite structure, namely, functionally graded FG graphene reinforced composite GRC coated plates/shells. A complex power law function is used to define the material's graduation. Investigations are conducted on Hardcore and Softcore coated FG plates/shells. The virtual work approach is used to perform the equilibrium equations, which are then solved using the Galerkin technique to account for various boundary conditions. With reliable published articles, the presented solution is validated. The effects of hardcore and softcore distributions, gradation indexes, and boundary conditions on the buckling, bending deflection and stresses of FG GRC-coated shells are presented in detail. Obtained results and the developed procedure are supportive for design and manufacturing of FG-GRC coated plates/shells in several fields and industries e.g., aerospace, automotive, marine, and biomedical implants.
Keywords: buckling; deflection; FGM; Galerkin technique; graphene reinforced composite; stresses

1. Introduction

Carbon and Graphene nanomaterials and their products are broadly utilized as strengthening nanofillers in polymers to enhance and increase their mechanical, electrical and thermal responses under different loading and operating conditions (Rysaeva *et al*. 2020a, b), while keeping the valuable characteristics of polymers as large deformation, sustainability, stretchability, and good chemical and biological compatibility, Feng *et al*. (2017). Many experimental analyses have reported that graphene-reinforced nanocomposites have a substantial enhancement in mechanical behaviors as compared to carbon nanotube composites, (Stankovich *et al*. 2006, Eltaher *et al*. 2018).

Advanced functionally graded materials (FGMs), which are characterized by a continuous spatial gradient in both material composition and properties (Esen *et al*. 2021a, Mohamed *et al*. 2022, Al-Zahrani *et al*. 2022), are used in many engineering fields ranging from macro-scale (i.e., aerospace, automotive, civil, marine, and biomedical implants) to nanoscale as MEMS (Melaibari *et al*. 2022), shape memory alloys, thin films, and The research community, Zhao *et al*. (2022), and others have taken into consideration the mechanical response of FG-GPLRC plates under various loading situations since Yang *et al*. (2017) introduced the novel multilayer FG graphene platelets (GPLs) reinforced composites (FG-GPLRC).

Dai and Mishnaevsky (2014) developed a 3D computational model for damage and fracture mechanisms graphene/polymer interface composite structure. Sedighi and Daneshmand (2014) and Sedighi (2014) examined the static and dynamic pull-in instability of multi-walled CNT probes by He's iteration perturbation method. Shen *et al*. (2017) and Wu *et al*. (2017) studied thermal buckling and post-buckling of FG-GPLRC plates resting on an elastic foundation and subjected to in-plane temperature variation. Using higher-order shear deformation theory, Daikh and Megueni (2018) conducted an analytical analysis of the thermal buckling of sandwich FG plates. Based on Reddy's higher-order shear deformation, She *et al*. (2018) predicted wave propagation of FG porous non-local strain gradient nanobeams. Karami *et al*. (2019) examined forced resonance vibration of FG-GPLRC nanoplate by employing the Halpin–Tsai model while the rule of the mixture is used to calculate the effective Poisson's ratio and mass density. Daikh *et al*. (2019, 2020a) created a closed-form solution to predict the buckling loads and free vibration of FGM sandwich nanoplates due to heat conduction based on the NLSG theory.

Abazid *et al*. (2020) used nonlocal strain gradient theory (NLSG) and a quasi-3D plate theory to study wave propagation in FG-GPLRC nanoplates supported on an elastic base. By employing the NLSG theory, Bouadi *et al*.

*Corresponding author, Professor
E-mail: meltaher@kau.edu.sa; mohaeltaher@gmail.com

ISSN: 2287-237X (Print), 2287-2388 (Online)

(2018) and Safaei *et al*. (2019) investigated the buckling behavior of single-layered graphene sheets. Uzun *et al*. (2019) obtained the optimum cross-sectional dimensions of nanobeam elements based on Bernoulli beam model and nonlocal elasticity theory. The coupled electromechanical governing equation of the smart interdisciplinary porous plate with piezoceramic faces reinforced by CNT was developed by Moradi-Dastjerdi *et al*. (2020). Using the NLSG theory, Daikh *et al*. (2020b, c) investigated the mechanical reactions of composite nanoplates reinforced with FG carbon nanotubes. By taking into account the temperature-dependent material properties, Daikh *et al*. (2020d, e) examined the bending behavior of FG sandwich nanoplates supported by elastic foundations and the bending response of sandwich plates in a thermal environment. The thermal buckling characteristics of plates embedded with graphene-oxide powder were investigated by Ebrahimi *et al*. (2020). The impact of g GPLs and CNTs on the enhancement of mechanical properties in the stir-casting process of Al matrix nanocomposites was investigated by Hadad *et al*. (2020). Ghannadpour and Moradi (2020), Mehrez *et al*. (2020), and Shariati *et al*. have all looked at the vibrational behavior of nano-single-layer graphene sheets. Hamilton's principle was used by Eyvazian *et al*. (2020) to study the vibration response of a cylindrical FG-GNPRC nanoshell subjected to a moving harmonic load.

Ouakad *et al*. (2020) presented the effects of material properties, nonlocal parameter, Lorentz and electric forces on natural frequencies of actuated hybrid carbon/boron-nitride subjected to thermal loads. Zhao *et al*. (2020) presented research activities and a comprehensive review of FG-GPLRC structures and existing micromechanics models to predict the effective mechanical properties of GPLRC. Shariati *et al*. (2020) studied stability and dynamics of viscoelastic moving Rayleigh beams with an asymmetrical distribution of material parameters. Qin *et al*. (2020) used several numerical techniques to establish a 3D solution for the free vibration of FG-GPLRC cylindrical shells resting on elastic foundations. Bensaid *et al*. (2020) investigated how FG nanobeam vibration and buckling were affected by microstructure defects. Sedighi *et al*. (2020) exploited the Stress-driven nonlocal elasticity in analysing the instability analysis of fluid-conveying C-BN hybrid-nanotube in a magneto-thermal environment.

Modified couple stress theory (MCST) and NLSG theory were both used by Abdelrahman *et al*. (2021a, b) to explore numerically via the FEM the dynamic vibration of perforated Timoshenko microbeams under accelerating dynamic loads and the thermal environment. Based on the new quasi-3D hyperbolic shear deformation theory, Lu *et al*. (2021a, b) assessed the post-buckling, free vibration, and dynamic stability of FG composite multilayer microtubes reinforced by GNPLs. Koochi and Goharimanesh (2021) studied the nonlinear oscillation of carbon nanotube manufactured nano-resonator in the context of the nonlocal elasticity. Esmaeilzadeh *et al*. (2021) studied the thermo-mechanical comportment of GRC moving polymer nanoplates. Esen *et al*. (2021b) presented the impact of microstructure and size-scale on the free vibration and stability of FG nanobeams exposed to magnetic and thermal environments with and without cracks using the NLSG theory. Based on the Halpin-Tsai model and Timoshenko beam theory, She *et al*. (2021) investigated the forced vibration response of curved microbeams reinforced by graphene nanoplatelets (GNPs). Using an improved finite shell element, Zghal *et al*. (2021) investigated the thermal vibration response of FG plates and panels. The snap-buckling and vibration responses of the Functionally graded GPLRC's beams resting on the elastic foundations and subjected to a thermal environment were anticipated by Zhang *et al*. (2022).

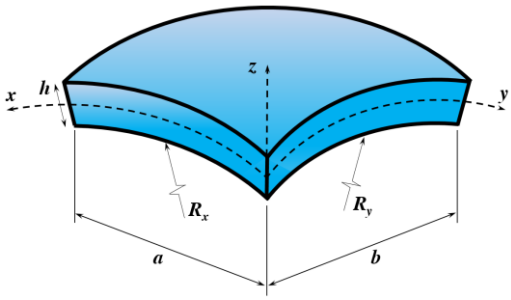

Fig. 1 Tri-coated FG spherical shell geometry

According to the listed literature and the best of authors' knowledge analysis of buckling stability as well as bending behavior of coated functionally graded (FG) graphene-reinforced composite (GRC) shells, has not been handled elsewhere. In the following research, we present a comprehensive study to investigate the buckling stability and bending deflection of composite shells reinforced by graphene, namely coated functionally graded (FG) graphene-reinforced composite (GRC), five GPLs distribution patterns are considered. The rest of this study is organized as, section 2 illustrates the material distribution and graduation functions with Halpin–Tsai model. Governing equations on the basis of generalized shear deformation plate theory are presented in sections 3 and 4. Analytical solutions and admissible boundary conditions are illustrated in section 5. The model verification and numerical parametric studies are developed in section 6. Conclusions and main points are summarized in section 7.

2. Material distribution and graduation

Consider a composite shell of length a, width b and thickness h (see Fig. 1). The principal curvature radii of the shell midplane in x and y directions are R_x and R_y, respectively. The studied structure is made from an epoxy matrix reinforced by graphene nanoplatelets (GPLs). The weight fraction of GPLs varies in the three directions of the shell. Two types of FG GRNC shells are presented, hardcore FG shells and softcore FG shells. As presented in Fig. 1b, five patterns of GPLs distribution are considered, tridirectionally material distribution pattern (FG-A GRC), two bidirectional material distribution patterns (FG-B GRC and FG-C GRC), unidirectional transverse material distribution (FG-D GRC) and unidirectional axial material distribution (FG-E GRC).

Young's modulus (E) and Poisson's ratio (υ), can be expressed by the law of mixture as

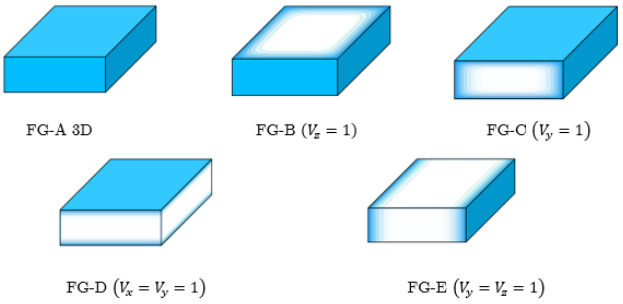

Fig. 2 Various schemes of coated FG shell $(R_x = R_y = \infty)$

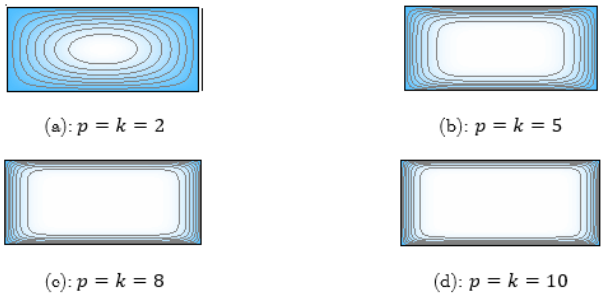

Fig. 3 Functionally graded material distribution

$$P(x,y,z) = P_m + (P_e - P_m)V(x,y,z) \tag{1}$$

where P_p and P_e are the mechanical properties of the matrix and the effective material properties of matrix /GPL constituents, respectively. The volume fraction $V(x,y,z)$ of matrix /GPL phase in both x, y and z directions, and is given using three functions as, (Abdelhaffez *et al*. 2023)

$$\begin{cases} V(x) = \left[\left(\dfrac{|2x-a|}{a}\right)^k - 1\right] \\ V(x) = \left[\left(\dfrac{|2y-b|}{b}\right)^k - 1\right] \\ V(z) = \left[\left(\dfrac{|2z|}{h}\right)^p - 1\right] \end{cases} \tag{2}$$

The total volume fraction of the Hardcore (HC) coated FG-GRC shell, can be expressed as:

$$V(x,y,z) = V(x)V(y)V(z) \tag{3}$$

and for the Softcore (SC) coated FG-GRC shell (as shown in Figs. 2 and 3):

$$V(x,y,z) = 1 - V(x)V(y)V(z) \tag{4}$$

By employing Halpin–Tsai mixture model, the effective Young's modulus of the shell is expressed as, Affdl and Kardos (1976)

$$E_e = \frac{3}{8}\frac{1+\xi_{\mathrm{L}}\eta_{\mathrm{L}}V_{GPL}}{1-\eta_{\mathrm{L}}V_{GPL}}E_m + \frac{5}{8}\frac{1+\xi_{\mathrm{W}}\eta_{\mathrm{W}}V_{GPL}}{1-\eta_{\mathrm{W}}V_{GPL}}E_m \tag{5}$$

where

$$\eta_{\mathrm{L}} = \frac{(E_{\mathrm{GPL}}/E_m)-1}{(E_{\mathrm{GPL}}/E_m)+\xi_{\mathrm{L}}} \tag{6}$$

$$\eta_{\mathrm{W}} = \frac{(E_{\mathrm{GPL}}/E_m)-1}{(E_{\mathrm{GPL}}/E_m)+\xi_{\mathrm{W}}} \tag{7}$$

$$\xi_{\mathrm{L}} = 2\left(\frac{a_{\mathrm{GPL}}}{h_{\mathrm{GPL}}}\right) \tag{8}$$

$$\xi_{\mathrm{W}} = 2\left(\frac{b_{\mathrm{GPL}}}{h_{\mathrm{GPL}}}\right) \tag{9}$$

The effective Poisson's ratio υ_{e} of the epoxy/GPL phase is expressed as follows:

$$\upsilon_{\mathrm{e}} = \upsilon_{\mathrm{GPL}}V_{GPL} + \upsilon_{\mathrm{m}}V_{\mathrm{m}} \tag{10}$$

υ_{GPL} and υ_{m} are Poisson's ratio of the GPLs and the matrix. V_{GPL} and V_m where the GPLs and the matrix volume fraction, respectively, where:

$$V_{GPL} = \frac{W_{GPL}}{W_{GPL} + (\rho_{\mathrm{GPL}}/\rho_{\mathrm{m}})(1-W_{\mathrm{GPL}})} \tag{11}$$

and

$$V_m = 1 - V_{GPL} \tag{12}$$

where W_{GPL} is the total GPLs weight fraction.

3. Mathematical formulations

In the current analysis, a hyperbolic sine function shear deformation theory is used to obtain the equilibrium equations for the static response of coated FG GRC shells. The displacement field is given as

$$\begin{aligned} u(x,y,z,t) &= \left(1+\frac{z}{R_x}\right)u_0 - z\frac{\partial w_0}{\partial x} + f(z)\psi_x \\ v(x,y,z,t) &= \left(1+\frac{z}{R_y}\right)v_0 - z\frac{\partial w_0}{\partial y} + f(z)\psi_y \\ w(x,y,z,t) &= w_0 \end{aligned} \tag{13}$$

The midplane displacements of the shell are u_0, v_0, and w_0. ψ_x and ψ_y are the transverse normal rotations at $z = 0$. The shape function $f(z)$ is given as

$$f(z) = h\sinh\left(\frac{z}{h}\right) - \frac{3z^3}{2h^2} \tag{14}$$

The strains can be given from the above displacement as

$$\begin{Bmatrix} \varepsilon_{xx} \\ \varepsilon_{yy} \\ \gamma_{xy} \end{Bmatrix} = \begin{Bmatrix} \varepsilon^0_{xx} \\ \varepsilon^0_{yy} \\ \gamma^0_{xy} \end{Bmatrix} + z\begin{Bmatrix} \varepsilon^1_{xx} \\ \varepsilon^1_{yy} \\ \gamma^1_{xy} \end{Bmatrix} + f(z)\begin{Bmatrix} \varepsilon^2_{xx} \\ \varepsilon^2_{yy} \\ \gamma^2_{xy} \end{Bmatrix}$$
$$\varepsilon_{zz} = 0, \quad \begin{Bmatrix} \gamma_{yz} \\ \gamma_{xz} \end{Bmatrix} = \frac{\mathrm{d}f(z)}{\mathrm{d}z}\begin{Bmatrix} \gamma^0_{yz} \\ \gamma^0_{xz} \end{Bmatrix}, \tag{15}$$

where

$$\begin{Bmatrix} \varepsilon^0_{xx} \\ \varepsilon^0_{yy} \\ \gamma^0_{xy} \end{Bmatrix} = \begin{Bmatrix} \dfrac{\partial u_0}{\partial x} + \dfrac{w_0}{R_x} \\ \dfrac{\partial v_0}{\partial y} + \dfrac{w_0}{R_y} \\ \dfrac{\partial v_0}{\partial x} + \dfrac{\partial u_0}{\partial y} \end{Bmatrix}, \quad \begin{Bmatrix} \varepsilon^1_{xx} \\ \varepsilon^1_{yy} \\ \gamma^1_{xy} \end{Bmatrix} = -\begin{Bmatrix} \dfrac{\partial^2 w_0}{\partial x^2} \\ \dfrac{\partial^2 w_0}{\partial y^2} \\ 2\dfrac{\partial^2 w_0}{\partial x \partial y} \end{Bmatrix},$$
$$\begin{Bmatrix} \varepsilon^2_{xx} \\ \varepsilon^2_{yy} \\ \gamma^2_{xy} \end{Bmatrix} = \begin{Bmatrix} \dfrac{\partial \varphi_1}{\partial x} \\ \dfrac{\partial \varphi_2}{\partial y} \\ \dfrac{\partial \varphi_2}{\partial x} + \dfrac{\partial \varphi_1}{\partial y} \end{Bmatrix}, \quad \begin{Bmatrix} \gamma^0_{yz} \\ \gamma^0_{xz} \end{Bmatrix} = \begin{Bmatrix} \varphi_x \\ \varphi_y \end{Bmatrix}. \tag{16}$$

The stresses relations related to the strains can be portrayed as, (Assie *et al*. 2023)

$$\begin{Bmatrix}\sigma_{xx}\\ \sigma_{yy}\\ \tau_{yz}\\ \tau_{xz}\\ \tau_{xy}\end{Bmatrix}=\begin{bmatrix}Q_{11} & Q_{12} & 0 & 0 & 0\\ Q_{12} & Q_{22} & 0 & 0 & 0\\ 0 & 0 & Q_{44} & 0 & 0\\ 0 & 0 & 0 & Q_{55} & 0\\ 0 & 0 & 0 & 0 & Q_{66}\end{bmatrix}\begin{Bmatrix}\varepsilon_{xx}\\ \varepsilon_{yy}\\ \gamma_{yz}\\ \gamma_{xz}\\ \gamma_{xy}\end{Bmatrix} \tag{17}$$

where

$$Q_{11}=\frac{E}{1-\nu^2}\,,\qquad Q_{22}=Q_{11}\,,\qquad Q_{12}=\frac{\nu E}{1-\nu^2},\\ Q_{44}=Q_{55}=Q_{66}=\frac{E}{2(1+\nu)} \tag{18}$$

The stress relations, moment and additional moment resultants can obtain by the integration of Eq. (17) as

$$\begin{Bmatrix}\{N\}\\ \{M\}\\ \{P\}\end{Bmatrix}=\begin{bmatrix}[A] & [B] & [C]\\ [B] & [D] & [F]\\ [C] & [F] & [H]\end{bmatrix}\begin{Bmatrix}\{\varepsilon^0\}\\ \{\varepsilon^1\}\\ \{\varepsilon^2\}\end{Bmatrix} \tag{19}$$

$$\begin{Bmatrix}R_{yz}\\ R_{xz}\end{Bmatrix}=\begin{bmatrix}J_{44} & J_{45}\\ J_{45} & J_{55}\end{bmatrix}\begin{Bmatrix}\gamma^0_{yz}\\ \gamma^0_{xz}\end{Bmatrix} \tag{20}$$

where

$$\begin{aligned}\{N\}&=\{N_{xx}\quad N_{yy}\quad N_{xy}\}^T\\ \{M\}&=\{M_{xx}\quad M_{yy}\quad M_{xy}\}^T\\ \{P\}&=\{P_{xx}\quad P_{yy}\quad P_{xy}\}^T\\ \{\varepsilon^0\}&=\{\varepsilon^0_{xx}\quad \varepsilon^0_{yy}\quad \gamma^0_{xy}\}^T\\ \{\varepsilon^1\}&=\{\varepsilon^1_{xx}\quad \varepsilon^1_{yy}\quad \gamma^1_{xy}\}^T\\ \{\varepsilon^2\}&=\{\varepsilon^2_{xx}\quad \varepsilon^2_{yy}\quad \gamma^2_{xy}\}^T\end{aligned} \tag{21}$$

and

$$\{A_{ij},B_{ij},D_{ij},C_{ij},F_{ij},H_{ij}\}=\sum_{n=1}^{n}\int_{h_{n-1}}^{h_n}Q_{ij}{}^{(n)}\{1,z,z^2,f(z),zf(z),f(z)^2\}\mathrm{d}z\,,\quad (i,j=1,2,6)\\ J_{ii}=\sum_{n=1}^{n}\int_{h_{n-1}}^{h_n}Q_{ii}{}^{(n)}\left[\frac{\mathrm{d}f(z)}{\mathrm{d}z}\right]^2\mathrm{d}z\,,(i=4,5) \tag{22}$$

4. Equilibrium equations

The variation of the strain energy of the composite shell can be expressed as

$$\delta U_p=\frac{1}{2}\int_V\begin{bmatrix}\sigma_{xx}^{(k)}\delta\varepsilon_{xx}+\sigma_{yy}^{(k)}\delta\varepsilon_{xx}+\sigma_{xy}^{(k)}\delta\gamma_{xy}\\ +\sigma_{xz}^{(k)}\delta\gamma_{xz}+\sigma_{yz}^{(k)}\delta\gamma_{yz}\end{bmatrix}\mathrm{d}V\\ -\frac{1}{2}\int_A[q\delta w]\mathrm{d}A \tag{23}$$

Here, q presents the external transverse applied load. The equilibrium equations of the FG GRC shell can be calculated as follows:

$$A_{11}\frac{\partial^2u_0}{\partial x^2}+A_{66}\frac{\partial^2u_0}{\partial y^2}+(A_{12}+A_{66})\frac{\partial^2v_0}{\partial x\partial y}\\ +\left(\frac{A_{11}}{R_x}+\frac{A_{12}}{R_y}\right)\frac{\partial w_0}{\partial x}-B_{11}\frac{\partial^3w_0}{\partial x^3}-(B_{12}+2B_{66})\frac{\partial^3w_0}{\partial x\partial y^2}\\ +B^s_{11}\frac{\partial^2\psi_x}{\partial x^2}+B^s_{66}\frac{\partial^2\psi_x}{\partial y^2}+(B^s_{12}+B^s_{66})\frac{\partial^2\psi_y}{\partial x\partial y}=0 \tag{24}$$

$$(A_{12}+A_{66})\frac{\partial^2u_0}{\partial x\partial y}+A_{22}\frac{\partial^2v_0}{\partial y^2}+A_{66}\frac{\partial^2v_0}{\partial x^2}\\ -(B_{12}+2B_{66})\frac{\partial^3w_0}{\partial x^2\partial y}-B_{22}\frac{\partial^3w_0}{\partial y^3}+\left(\frac{A_{12}}{R_x}+\frac{A_{22}}{R_y}\right)\frac{\partial w_0}{\partial x}\\ +(B^s_{12}+B^s_{66})\frac{\partial^2\psi_x}{\partial x\partial y}+B^s_{22}\frac{\partial^2\psi_y}{\partial y^2}+B^s_{66}\frac{\partial^2\psi_y}{\partial x^2}=0 \tag{25}$$

$$B_{11}\frac{\partial^3u_0}{\partial x^3}+(B_{12}+2B_{66})\frac{\partial^3u_0}{\partial x\partial y^2}-\left(\frac{A_{11}}{R_x}+\frac{A_{12}}{R_y}\right)\frac{\partial u_0}{\partial x}\\ +(B_{12}+2B_{66})\frac{\partial^3v_0}{\partial x^2\partial y}+B_{22}\frac{\partial^3v_0}{\partial y^3}-\left(\frac{A_{12}}{R_x}+\frac{A_{22}}{R_y}\right)\frac{\partial v_0}{\partial y}\\ +\left(\frac{2B_{11}}{R_x}+\frac{2B_{12}}{R_y}\right)\frac{\partial^2w_0}{\partial x^2}-D_{11}\frac{\partial^4w_0}{\partial x^4}\\ -(2D_{12}+4D_{66})\frac{\partial^4w_0}{\partial x^2\partial y^2}-D_{22}\frac{\partial^4w_0}{\partial y^4}\\ +\left(\frac{2B_{12}}{R_x}+\frac{2B_{22}}{R_y}\right)\frac{\partial^2w_0}{\partial y^2}-\left(\frac{A_{11}}{{R_x}^2}+2\frac{A_{12}}{R_xR_y}+\frac{A_{22}}{{R_y}^2}\right)w_0\\ +D^s_{11}\frac{\partial^3\psi_x}{\partial x^3}+(D^s_{12}+2D^s_{66})\frac{\partial^3\psi_x}{\partial x\partial y^2}-\left(\frac{B^s_{11}}{R_x}+\frac{B^s_{12}}{R_y}\right)\frac{\partial\psi_x}{\partial x}\\ +(D^s_{12}+2D^s_{66})\frac{\partial^3\psi_y}{\partial x^2\partial y}+D^s_{22}\frac{\partial^3\psi_y}{\partial y^3}-\left(\frac{B^s_{12}}{R_x}+\frac{B^s_{22}}{R_y}\right)\frac{\partial\psi_y}{\partial y}\\ +q+\bar{N}^0_{xx}\frac{\partial^2\mathrm{w}}{\partial x^2}+\bar{N}^0_{yy}\frac{\partial^2w_0}{\partial y^2}=0 \tag{26}$$

$$B^s_{11}\frac{\partial^2u_0}{\partial x^2}+B^s_{66}\frac{\partial^2u_0}{\partial y^2}+(B^s_{12}+B^s_{66})\frac{\partial^2v_0}{\partial x\partial y}-D^s_{11}\frac{\partial^3w_0}{\partial x^3}\\ -(D^s_{12}+2D^s_{66})\frac{\partial^3w_0}{\partial x\partial y^2}+\left(\frac{B^s_{11}}{R_x}+\frac{B^s_{12}}{R_y}\right)\frac{\partial w_0}{\partial x}+F^s_{11}\frac{\partial^2\psi_x}{\partial x^2}\\ +F^s_{66}\frac{\partial^2\psi_x}{\partial y^2}-A^s_{44}\psi_x+(F^s_{12}+F^s_{66})\frac{\partial^2\psi_y}{\partial x\partial y}=0 \tag{27}$$

$$(B^s_{12}+B^s_{66})\frac{\partial^2u_0}{\partial x\partial y}+B^s_{11}\frac{\partial^2v_0}{\partial y^2}+B^s_{66}\frac{\partial^2v_0}{\partial x^2}\\ -(D^s_{12}+2D^s_{66})\frac{\partial^3w_0}{\partial x^2\partial y}-D^s_{22}\frac{\partial^3w_0}{\partial y^3}+\left(\frac{B^s_{12}}{R_x}+\frac{B^s_{22}}{R_y}\right)\frac{\partial w_0}{\partial x}\\ +(F^s_{12}+F^s_{66})\frac{\partial^2\psi_x}{\partial x\partial y}+F^s_{11}\frac{\partial^2\psi_y}{\partial y^2}+F^s_{66}\frac{\partial^2\psi_y}{\partial x^2}-A^s_{44}\psi_y=0 \tag{28}$$

5. Analytical solution

To analyze various boundary conditions, Galerkin approach is used in this section to provide accurate solutions. The formulations of displacements can be written as:

$$\{u_0,\psi_x\}=\sum_{m=1}^{\infty}\sum_{n=1}^{\infty}\{U_{mn},X_{mn}\}\frac{\partial X_m(x)}{\partial x}Y_n(y)e^{i\omega t}\\ \{v_0,\psi_y\}=\sum_{m=1}^{\infty}\sum_{n=1}^{\infty}\{V_{mn},Z_{mn}\}X_m(x)\frac{\partial Y_n(y)}{\partial y}e^{i\omega t}\\ w_0=\sum_{m=1}^{\infty}\sum_{n=1}^{\infty}W_{mn}X_m(x)Y_n(y)\,e^{i\omega t} \tag{29}$$

Note that U_{mn}, V_{mn}, X_{mn} and Z_{mn} are arbitrary parameters. The functions $X_m(x)$ and $Y_n(y)$ that satisfy hinged and clamped boundary conditions are given in Table 1.

Table 1 The admissible functions $X_m(x)$ and $Y_n(y)$

BCs.	The functions X_m and Y_n	
	$X_m(x)$	$X_m(x)$
SSSS	$\sin(\alpha x)$	$\sin(\beta y)$
CCCC	$\sin^2(\alpha x)$	$\sin^2(\beta y)$
CSCS	$\sin(\alpha x)[\cos(\alpha x)-1]$	$\sin(\beta y)[\cos(\beta y)-1]$
CCSS	$\sin^2(\alpha x)$	$\sin(\beta y)$

Table 2 Comparison of dimensionless critical buckling load ($\times 10^{-2}$) of uniform distribution GRC plate under compressive uniaxial loads ($a=b=10h$, $a_{\mathrm{GPL}}=2.5$ μm, $\mathrm{h_{GPL}}=1.5$ nm, $\mathrm{w_{GPL}}=1.5$ μm)

W_{GPL} (%)	Sources				
	Wu *et al*. (2017)	Gholami (2019)	Thai *et al*. (2019)	Present	%Error
0.0	0.0310	0.0311	0.0309	0.0310	0.323625
0.1	0.0413	0.0414	0.0412	0.0413	0.242718
0.3	0.0619	0.0620	0.0618	0.0620	0.323625
0.5	0.0825	0.0826	0.0824	0.0827	0.364078
1.0	-	-	0.1338	0.1342	0.298954

Table 3 Comparison of dimensionless central deflection, normal stress and shear stress of homogenous plate ($b=a=10h, E_c=151\mathrm{GPa}, \nu_c=0.3$)

Source	Zenkour (2013) FSDT	Zenkour (2013) TSDT	Zenkour (2013) SSDT	Neves (2012)	Present	%Error
$\bar{w}$	0.19607	0.19606	0.19605	0.1961	0.19605	0
$\bar{\sigma}_{xx}$	1.97576	2.04985	2.05452	1.9947	2.05438	0.0068
$\bar{\tau}_{xz}$	0.19099	0.23857	0.24618	0.2538	0.24634	0.0650

where $\alpha=m\pi/a$, $\beta=n\pi/b$. m and n are mode numbers. The applied transverse sinusoidal load can be defined as:

$$q=-q_0\int_0^a\int_0^b \sin^2(\alpha x)\sin^2(\beta y)\,\mathrm{d}x\mathrm{d}y \tag{30}$$

where q_0 is the maximum load intensity.

By substituting Eq. (29) into Eq. (24-28), one obtains

$$\begin{bmatrix} K_{11} & K_{12} & K_{13} & K_{14} & K_{15} \\ K_{12} & K_{22} & K_{23} & K_{24} & K_{25} \\ K_{13} & K_{23} & K_{33} & K_{34} & K_{35} \\ K_{14} & K_{24} & K_{34} & K_{44} & K_{45} \\ K_{15} & K_{25} & K_{35} & K_{45} & K_{55} \end{bmatrix} \begin{Bmatrix} U_{mn} \\ V_{mn} \\ W_{mn} \\ \Psi_{mn} \\ \Phi_{mn} \end{Bmatrix} = \begin{Bmatrix} 0 \\ 0 \\ q \\ 0 \\ 0 \end{Bmatrix} \tag{31}$$

where the elements K_{ij} of the matrix of rigidity (K) are given in Appendix A.

6. Results and discussions

In this section, we proposed composite shell made of a mixture of epoxy and GPLs as matrix and reinforcement, respectively. The shell is exposed to axial loadings in one or two directions $\left(\bar{N}^0_{xx}=\chi_1 N_{cr},\ \bar{N}^0_{yy}=\chi_2 N_{cr}\right)$ for the buckling study, and transverse nonuniform (sinusoidal) loadings for the bending study. χ_1 and χ_2 are the axial loads intensities. The mechanical characteristics of epoxy and GPLs constituents are stated as, Epoxy (matrix): $E_m=3$ Gpa, $\nu_{\mathrm{m}}=0.34$, $\rho_m=1200\ \mathrm{kg/m^3}$. GPLs (reinforcement): $E_{\mathrm{GPL}}=1010$ Gpa, $\nu_{\mathrm{GPL}}=0.186$, $\rho_{\mathrm{GPL}}=1060\ \mathrm{kg/m^3}$. The proposed structure has a thickness $h=20\mathrm{nm}$, length $a=200\mathrm{nm}$ and width $b=200\mathrm{nm}$. The GNLs have a length $a_{\mathrm{GPL}}=3$ nm, thickness $\mathrm{h_{GPL}}=0.7$ nm and width $\mathrm{b_{GPL}}=1.8$ nm. The normalized results for buckling, displacements and stresses are computed with the following forms: Dimensionless critical buckling load: $\bar{N}=\frac{N_{cr}}{h^3}$, Dimensionless transverse displacements: $\bar{w}=\frac{10^2E_mh^3}{a^2q_0}w\left(\frac{a}{2},\frac{b}{2},z\right)$, Dimensionless stresses: $\bar{\sigma}_{xx}=\frac{ha}{q_0}\sigma_{xx}\left(\frac{a}{2},\frac{b}{2},\frac{h}{2}\right)$, $\bar{\tau}_{xz}=\frac{ha}{q_0}\tau_{xz}\left(0,\frac{b}{2},0\right)$.

6.1 Comparison study

Firstly, a comparison study was carried out to check the validation of our methodology. For the buckling problem, Table 2 is illustrated to validate our numerical results with the results obtained by Wu *et al* (2017), Gholami and Ansari (2019) and Thai *et al*. (2019). The analysed structure is FG graphene-reinforced composite straight plates with length and width $a=b=0.45\mathrm{m}$ and thickness $h=0.045\mathrm{m}$.

Furthermore, another validation is performed in Table 3 related to the dimensionless deflection, axial and shear stresses plate made of ceramic (Zirconia ZrO2). The obtained results are compared with the results of Zenkour (2013) using various plate theories and Neves *et al*. (2012) using zigzag theory. In general, it is worth noting that our results for both buckling, deflection and stresses are in excellent agreement with the other results.

6.1.1 Buckling analysis

The buckling behavior is analyzed in this section by varying various material and geometrical parameters. In Table 4, we present the impact of inhomogeneity parameters p, k and e which are varied from 1 to 10 on the dimensionless critical buckling load of FG-A GRC spherical shell subjected to a biaxial in-plane loading. In addition, under the same conditions, the effect of the weight fraction, various GPLs reinforcement patterns, the shell configuration and boundary conditions on the dimensionless critical buckling load of FG-A GRC spherical shell is presented in Tables 5 and 6.

For more details and clarity, Figs. 1-9 are plotted. Fig. 4 plotted the action of the inhomogeneity parameters p, k and e (p=$k=e$) and the material distribution patterns on the dimensionless critical buckling load of simply supported spherical FG-GRC shells. Two types of FG GRC shells are considered, Hardcore and softcore. For the hardcore shell, the augmentation of the parameters p, k and e render the shell stiffer, and leads to an increment in the critical buckling load regardless of the GPLs reinforcement patterns. The inverse effect is seen for the softcore. The inverse action is seen for the softcore shell. The case of hardcore shells with p=$k=e=0$ means that the shell is fully epoxy (absence of CNTs), and for softcore ones, the shell has the maximum proportion of CNTs with uniform distribution.

Table 4 Effect of inhomogeneity parameters on the dimensionless critical buckling load of FG-A GRC spherical shell subjected to a biaxial in-plane loading $\left(R_x/a = R_y/b = 5, SSSS, W_{GPL} = 1\%\right)$

k	e	p							
		Hardcore				Softcore			
		1	2	5	10	1	2	5	10
0	0	5,8668	5,8668	5,8668	5,8668	6,3537	6,3537	6,3537	6,3537
1	1	5,9028	5,9213	5,9472	5,9633	6,3177	6,2992	6,2733	6,2573
	2	5,9148	5,9394	5,9740	5,9954	6,3057	6,2810	6,2465	6,2251
	5	5,9268	5,9576	6,0008	6,0276	6,2937	6,2628	6,2196	6,1930
	10	5,9322	5,9658	6,0130	6,0422	6,2882	6,2546	6,2075	6,1783
2	1	5,9148	5,9394	5,9740	5,9954	6,3057	6,2810	6,2465	6,2251
	2	5,9308	5,9636	6,0098	6,0383	6,2896	6,2568	6,2107	6,1822
	5	5,9467	5,9878	6,0455	6,0811	6,2736	6,2325	6,1749	6,1394
	10	5,9540	5,9988	6,0617	6,1006	6,2663	6,2215	6,1587	6,1199
5	1	5,9268	5,9576	6,0008	6,0276	6,2937	6,2628	6,2196	6,1930
	2	5,9467	5,9878	6,0455	6,0811	6,2736	6,2325	6,1749	6,1394
	5	5,9667	6,0181	6,0902	6,1347	6,2535	6,2022	6,1302	6,0857
	10	5,9758	6,0318	6,1104	6,1591	6,2444	6,1884	6,1099	6,0614
10	1	5,9322	5,9658	6,0130	6,0422	6,2882	6,2546	6,2075	6,1783
	2	5,9540	5,9988	6,0617	6,1006	6,2663	6,2215	6,1587	6,1199
	5	5,9758	6,0318	6,1104	6,1591	6,2444	6,1884	6,1099	6,0614
	10	5,9856	6,0468	6,1326	6,1856	6,2345	6,1733	6,0877	6,0348

Table 5 Effect of the weigh fraction and the shell structure on the dimensionless critical buckling load of FG-A GRC spherical shell subjected to a biaxial in-plane loading $\left(R_x/a = R_y/b = 5, SSSS, p = k = e = 2\right)$

Struct.	W_{GPL} (%)	Hardcore					Softcore				
		FG-A	FG-B	FG-C	FG-D	FG-E	FG-A	FG-B	FG-C	FG-D	FG-E
Plate	0.0	5,2651	5,2651	5,2651	5,2651	5,2651	5,2651	5,2651	5,2651	5,2651	5,2651
	0.2	5,2801	5,3024	5,2883	5,3005	5,3217	5,3343	5,3120	5,3261	5,3139	5,2928
	0.6	5,3103	5,3774	5,3348	5,3715	5,4354	5,4733	5,4064	5,4488	5,4120	5,3484
	1.0	5,3408	5,4529	5,3817	5,4429	5,5499	5,6133	5,5014	5,5723	5,5106	5,4044
5 inf	0.0	5,4171	5,4171	5,4171	5,4171	5,4171	5,4171	5,4171	5,4171	5,4171	5,4171
	0.2	5,4329	5,4555	5,4414	5,4541	5,4753	5,4880	5,4654	5,4795	5,4667	5,4456
	0.6	5,4646	5,5327	5,4902	5,5285	5,5924	5,6306	5,5625	5,6050	5,5664	5,5029
	1.0	5,4965	5,6105	5,5392	5,6033	5,7103	5,7742	5,6604	5,7313	5,6668	5,5606
5 5	0.0	5,8730	5,8730	5,8730	5,8730	5,8730	5,8730	5,8730	5,8730	5,8730	5,8730
	0.2	5,8910	5,9148	5,9007	5,9151	5,9363	5,9492	5,9255	5,9396	5,9252	5,9040
	0.6	5,9272	5,9987	5,9562	5,9995	6,0634	6,1025	6,0310	6,0735	6,0299	5,9663
	1.0	5,9636	6,0832	6,0120	6,0845	6,1914	6,2568	6,1373	6,2082	6,1353	6,0291
10	0.0	5,2651	5,2651	5,2651	5,2651	5,2651	5,2651	5,2651	5,2651	5,2651	5,2651
	0.2	5,2801	5,3024	5,2883	5,3005	5,3217	5,3343	5,3120	5,3261	5,3139	5,2928
	0.6	5,3103	5,3774	5,3348	5,3715	5,4354	5,4733	5,4064	5,4488	5,4120	5,3484
	1.0	5,3408	5,4529	5,3817	5,4429	5,5499	5,6133	5,5014	5,5723	5,5106	5,4044

Table 6 Effect of boundary conditions on the dimensionless critical buckling load of FG-A GRC plate subjected to a biaxial in-plane loading $\left(W_{GPL}, p = k = e = 0\right)$

Struct.	BCs.	Hardcore					Softcore				
		FG-A	FG-B	FG-C	FG-D	FG-E	FG-A	FG-B	FG-C	FG-D	FG-E
Plate	SSSS	5,3408	5,4529	5,3817	5,4429	5,5499	5,6133	5,5014	5,5723	5,5106	5,4044

Plate	CCCC	13,0380	13,2970	13,1450	13,3060	13,5330	13,6720	13,4150	13,5640	13,4020	13,1780
	CCSS	9,6855	9,8808	9,7634	9,8801	10,0570	10,1640	9,9687	10,0850	9,9670	9,7929
	CSCS	10,3470	10,5560	10,4290	10,5540	10,7430	10,8580	10,6500	10,7750	10,6490	10,4620
5 inf	SSSS	5,4965	5,6105	5,5392	5,6033	5,7103	5,7742	5,6604	5,7313	5,6668	5,5606
	CCCC	13,4040	13,6670	13,5160	13,6830	13,9100	14,0510	13,7890	13,9380	13,7690	13,5450
	CCSS	9,8668	10,0640	9,9469	10,0670	10,2430	10,3510	10,1540	10,2700	10,1490	9,9748
	CSCS	10,5540	10,7650	10,6390	10,7670	10,9570	11,0730	10,8610	10,9860	10,8570	10,6700
5 5	SSSS	5,9636	6,0832	6,0120	6,0845	6,1914	6,2568	6,1373	6,2082	6,1353	6,0291
	CCCC	13,9780	14,2470	14,0960	14,2730	14,5010	14,6430	14,3740	14,5240	14,3440	14,1210
	CCSS	10,4440	10,6490	10,5310	10,6620	10,8380	10,9480	10,7440	10,8600	10,7280	10,5540
	CSCS	10,9090	11,1250	10,9980	11,1330	11,3220	11,4390	11,2240	11,3490	11,2130	11,0260
10	SSSS	5,3408	5,4529	5,3817	5,4429	5,5499	5,6133	5,5014	5,5723	5,5106	5,4044
	CCCC	13,5630	13,8270	13,6760	13,8460	14,0730	14,2140	13,9500	14,1000	13,9280	13,7040
	CCSS	10,1080	10,3080	10,1910	10,3150	10,4910	10,6000	10,4000	10,5160	10,3900	10,2160
	CSCS	10,6140	10,8260	10,7000	10,8290	11,0190	11,1340	10,9220	11,0480	10,9170	10,7300

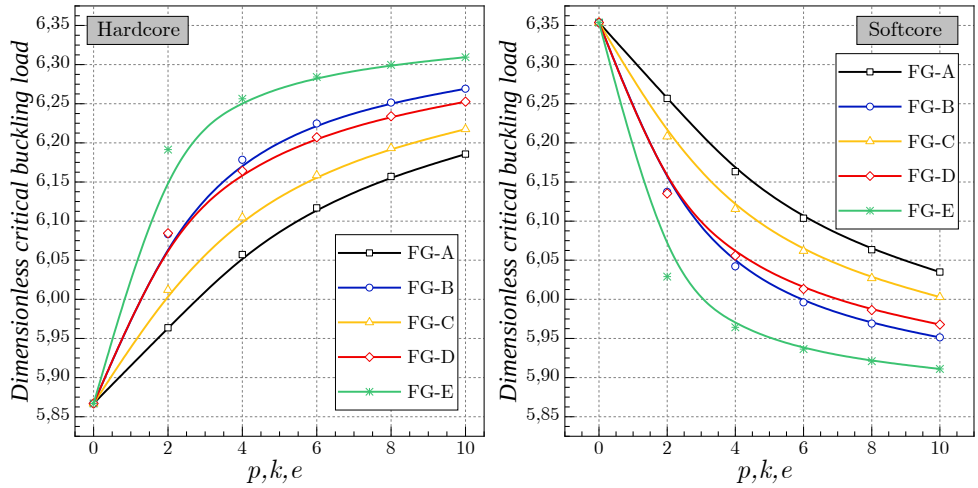

Fig. 4 Effect of the inhomogeneity parameters p, k and e on the dimensionless critical buckling load of various types of spherical FG-GRC shells $(SSSS, R_x/a = R_y/b = 5, W_{GPL} = 1\%)$

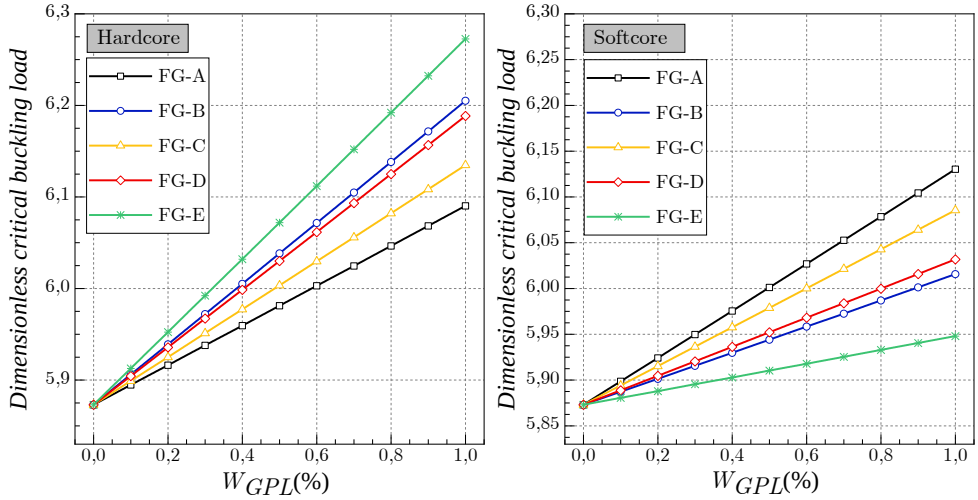

Fig. 5 Influence of weight faction variation on dimensionless critical buckling load of spherical FG-GRC shell for various GPLs reinforcement patterns $(R_x/a = R_y/b = 5, SSSS, p = k = e = 5)$

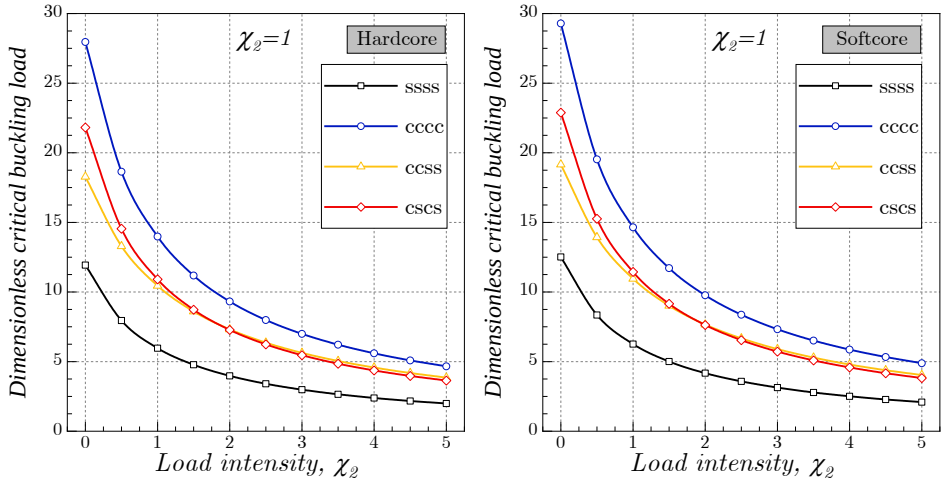

Fig. 6 Effect of the compressive inplane load intensity χ_2 and boundary conditions on the dimensionless critical buckling load of coated spherical GRC shells $(p = k = e = 2, R_x/a = R_y/b = 5, W_{GPL} = 1\%)$

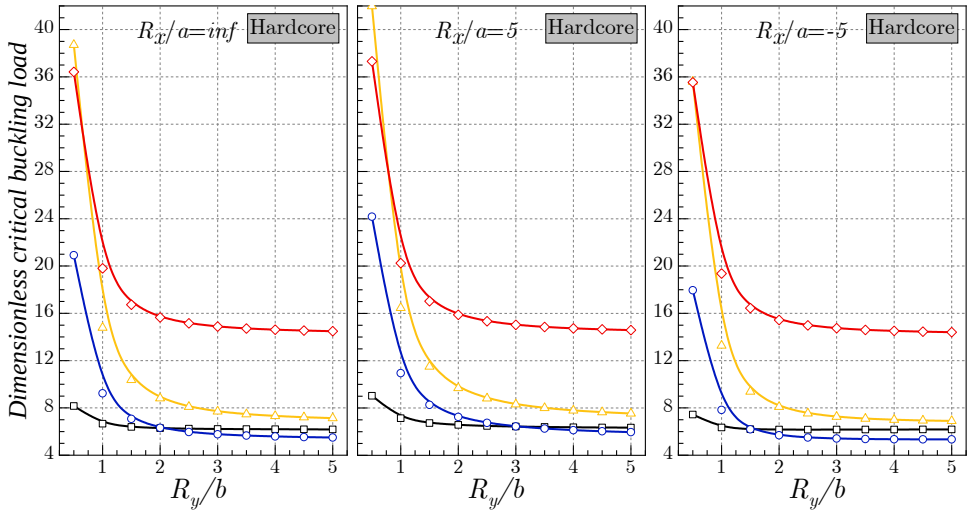

Fig. 7 Effect of the radius of curvature on the dimensionless critical buckling load of hardcore coated FG-A GRC shells $(SSSS, p = k = e = 2, b, W_{GPL} = 1\%)$

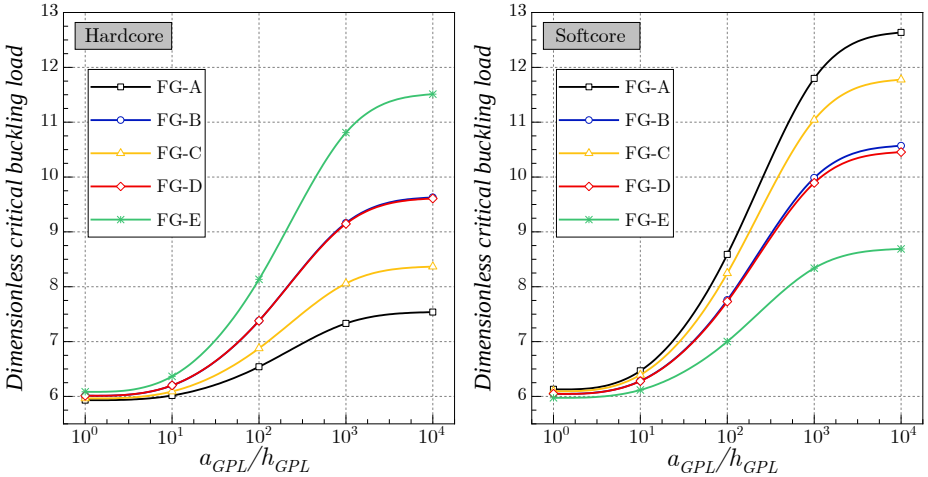

Fig. 8 Dimensionless critical buckling load of spherical FG GRC shell versus the length-to-thickness ratio of the GPLs nanofillers $(SSSS\ ,\ p = k = e = 2, W_{GPL} = 1\%)$

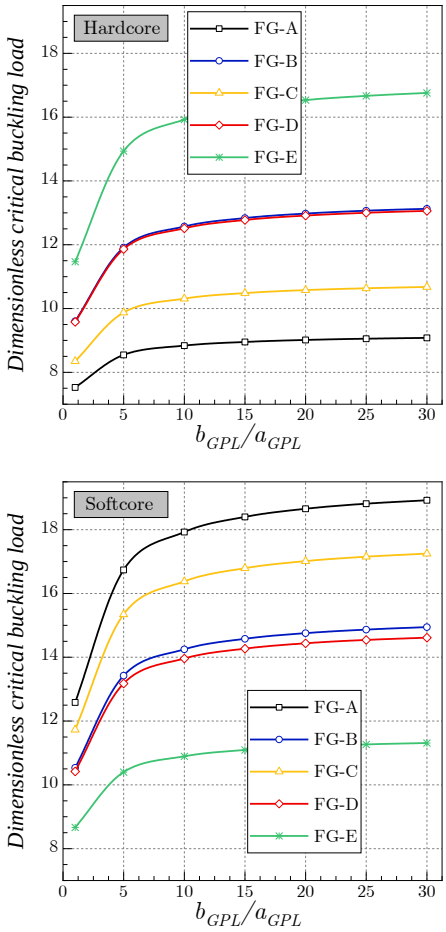

Fig. 9 Dimensionless critical buckling load of spherical FG GRC shell versus the width-to-length ratio of the GPLs nanofillers ($SSSS$, $p = k = e = 2, W_{GPL} = 1\%, a_{\mathrm{GPL}}/h_{\mathrm{GPL}} = 10^2$)

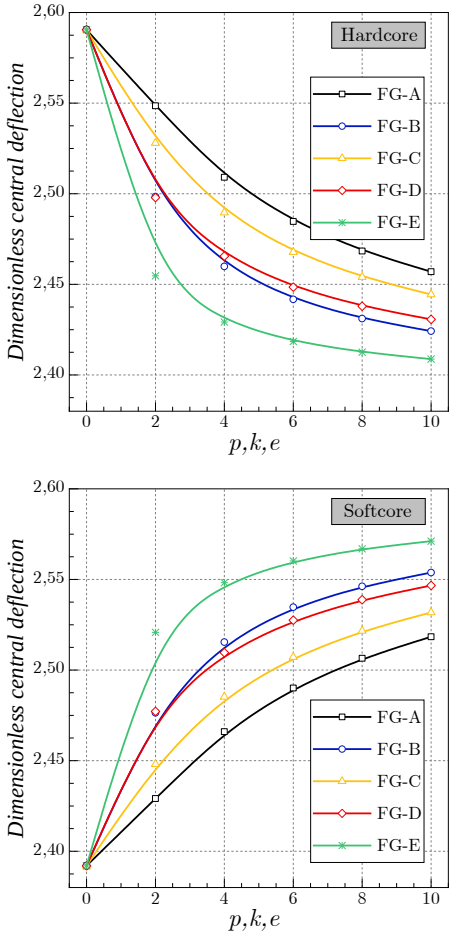

Fig. 10 Effect of the inhomogeneity parameters p, k and e on the dimensionless central deflection of various types of spherical GRC shells ($SSSS, R_x/a = R_y/b = 5, W_{GPL} = 1\%$)

The effect of the weight faction W_{GPT} (%) variation on dimensionless critical buckling load of spherical FG-GRC shell for various GPLs reinforcement patterns is plotted in Fig. 5. The increase of weight faction improves the shell stiffness, therefore, the critical buckling load increase, especially for the softcore shell case. Fig. 6 plots the impact of various boundary conditions and the compressive inplane load intensity χ_2 on the dimensionless critical buckling load of coated spherical GRC shells. It is clear that the increase in the load intensity χ_2 decrease the needed loads to buckle, wherever the boundary condition is. Moreover, the fully clamped shell (CCCC) has the highest values of the critical buckling loads because of its high rigidity than the other shells. Whereas the softer one is the simply supported shell.

In Fig. 7, the influence of the variation of the radius of curvature R_y/b on the dimensionless critical buckling load of hardcore coated FG-A GRC shells for various aspect ratios b/a ($b/a = 0.5, 1, 2, 5$) and the radius of curvature R_x/a ($R_x/a = inf, 5, -5$). It is observed that the increase of R_y/b leads to a decrease in the buckling loads for values $R_y/b < 2$, and then, for values more than two, all results are almost constant regardless of the aspect ratio. The critical buckling load of spherical FG GRC shells is presented in Figure 4 by varying the length-to-width ratio of GPL nanofillers. Various GPLs reinforcement patterns are considered. Regardless of the reinforcement pattern, it is clear that the augmentation in the thickness-to-length ratio $a_{\mathrm{GPL}}/h_{\mathrm{GPL}}$ increase critical buckling load.

To better explain the action of the geometry of the GPLs, the effect of the width-to-length ratio $b_{\mathrm{GPL}}/a_{\mathrm{GPL}}$ critical buckling load is depicted in Fig. 9. The obtain curves show that a significant effect of the width-to-length ratio on the critical buckling load is observed, where critical buckling load increase for values less than five ($b_{\mathrm{GPL}}/a_{\mathrm{GPL}} \leq 5$), and for the greater ratio values of $b_{\mathrm{GPL}}/\ a_{\mathrm{GPL}}$, the results are almost constant whatever GPLs reinforcement pattern is.

6.1.2 Bending analysis:

Fig. 10 plotted the action of the inhomogeneity parameters p, k and e (p=$k = e$) and the GPLs reinforcement patterns on the dimensionless central deflection of the two types of simply supported spherical FG-GRC shells, Hardcore and softcore. For the hardcore shell, the augmentation of the parameters p, k and e

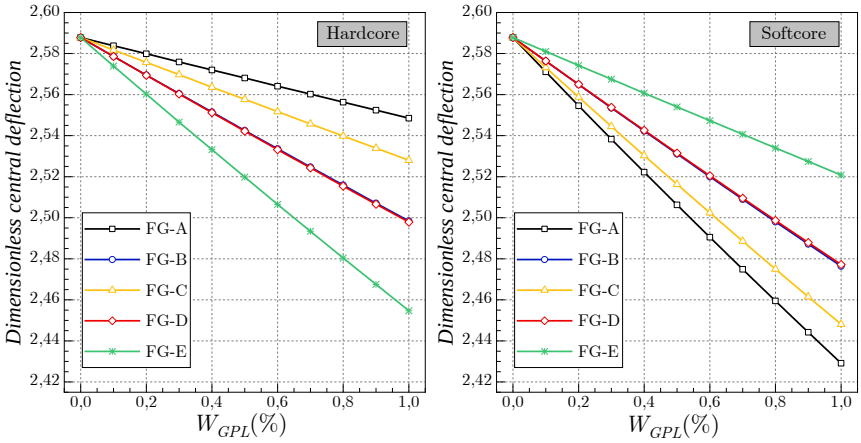

Fig. 11 Influence of weight faction variation on dimensionless central deflection of spherical FG-GRC shell for various GPLs reinforcement patterns $(SSSS, p = k = e = 2)$

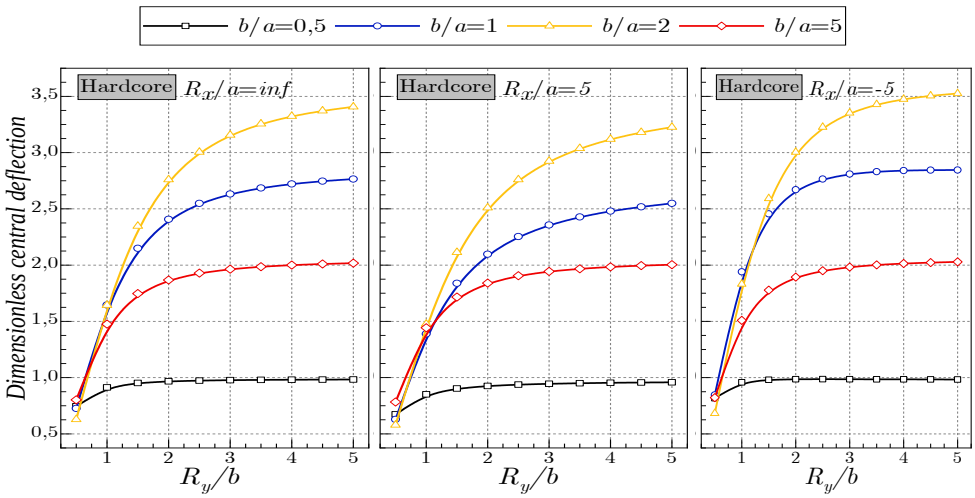

Fig. 12 Effect of the radius of curvature on the dimensionless central deflection of hardcore coated FG-A GRC shells $(SSSS, p = k = e = 2,\ W_{GPL} = 1\%)$

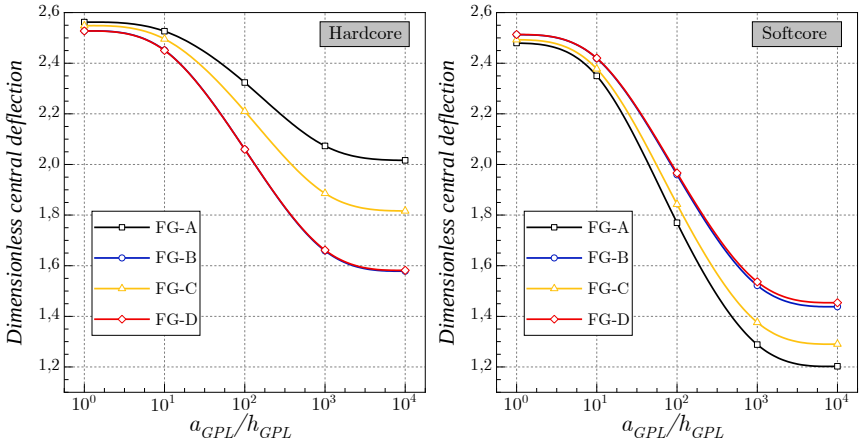

Fig. 13 Dimensionless central deflection of spherical GRC shell versus the length-to-thickness ratio of the GPLs nanofillers $(SSSS, g^*_{GPL} = 1\%)$

increase rigidity of the shell, therefore, the deflection of the shell is minimized. This effect is seen for all the GPLs reinforcement patterns. The inverse effect is seen for the softcore. The case of hardcore shells with p=$k = e = 0$ means that the shell is fully epoxy, without of CNTs, and for softcore one, the shell has the maximum proportion of

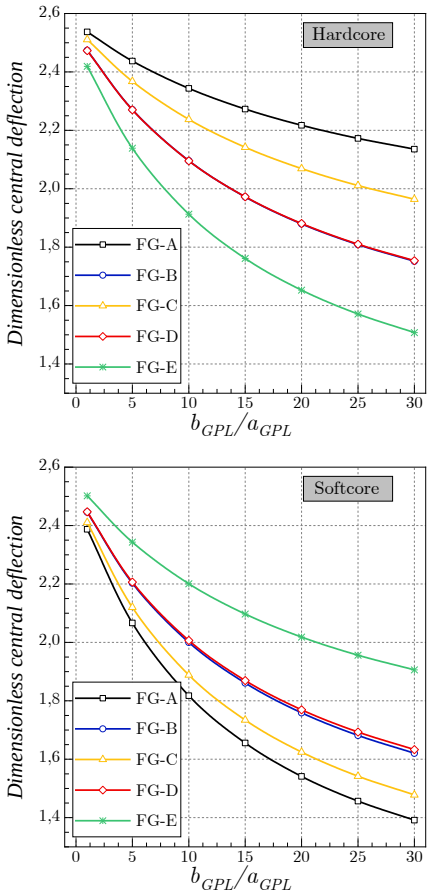

Fig. 14 Dimensionless central deflection of spherical FG GRC shell versus the width-to-length ratio of the GPLs nanofillers $(SSSS, p = k = e = 2, W_{GPL} = 1\%, a_{\mathrm{GPL}}/h_{\mathrm{GPL}} = 10^2)$

CNTs with uniform distribution, and this can explain the minimum and the maximum deflection in fully epoxy shell and uniform GPLs distribution shell, respectively.

Fig. 10 plotted the action of the inhomogeneity parameters p, k and e ($p = k = e$) and the GPLs reinforcement patterns on the dimensionless central deflection of the two types of simply-supported spherical FG-GRC shells, Hardcore and softcore. For the hardcore shell, the augmentation of the parameters p, k and e increase rigidity of the shell, therefore, the deflection of the shell is minimized. This effect is seen for all the GPLs reinforcement patterns. The inverse effect is seen for the softcore. The case of hardcore shells with p=$k = e = 0$ means that the shell is fully epoxy, without of CNTs, and for softcore ones, the shell has the maximum proportion of CNTs with uniform distribution, and this can explain the minimum and the maximum deflection in fully epoxy shell and uniform GPLs distribution shell, respectively.

The influence of the weight fraction W_{GPT} (%) variation on the dimensionless central deflection of spherical FG-GRC shell for various GPLs reinforcement patterns is plotted in Fig. 11. Unlike softcore shells, among various patterns of hardcore shells, the rigid shell is the FG-A shell, while the soft one is the FG-E shell. The increase in weight faction improves the shell stiffness, and for that, the deflections decrease.

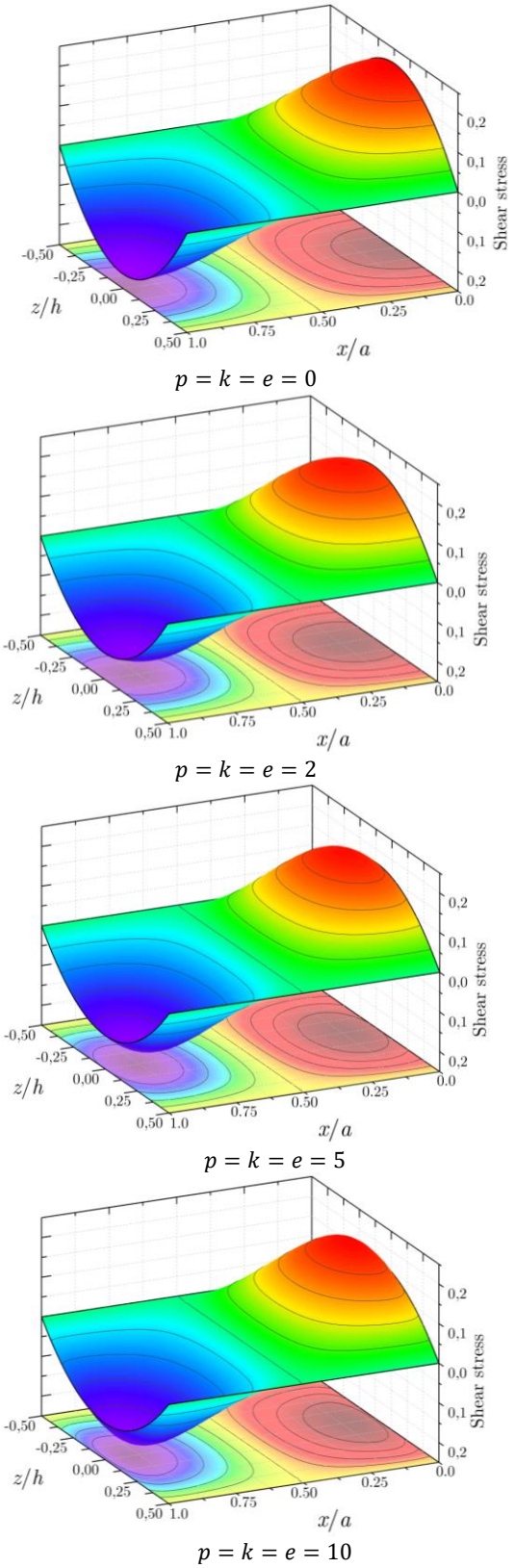

Fig. 15 Dimensionless axial stresses $\bar{\sigma}_{xx}$ of hardcore coated spherical FG-A GRC shell $(SSSS, W_{GPL} = 5\%)$

The influence of the variation of the radius of curvature R_y/b on the dimensionless deflection of hardcore coated FG-A GRC shells for various aspect ratios b/a and radius

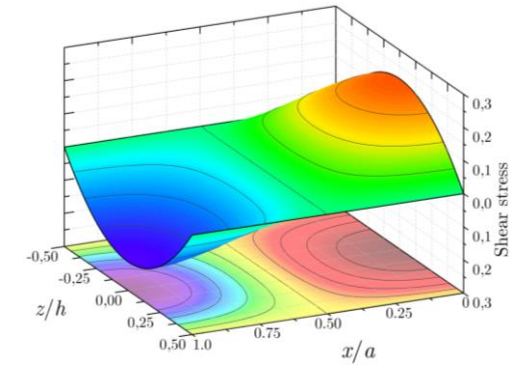

$p = k = e = 0$

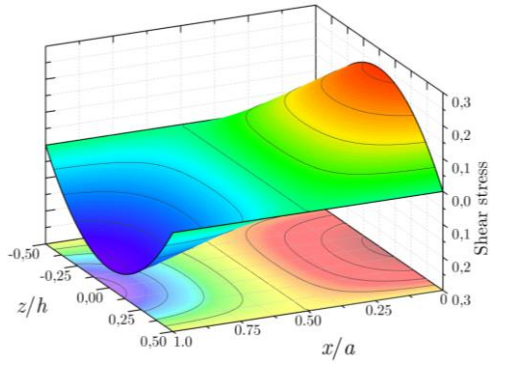

$p = k = e = 2$

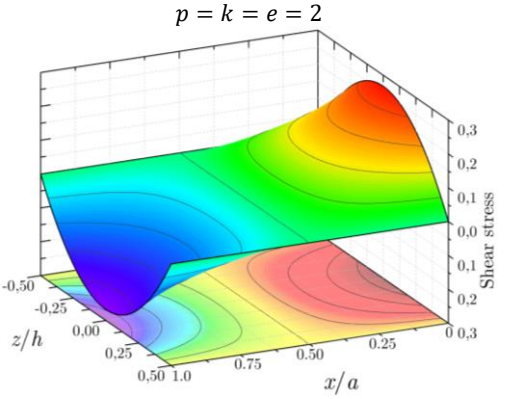

$p = k = e = 5$

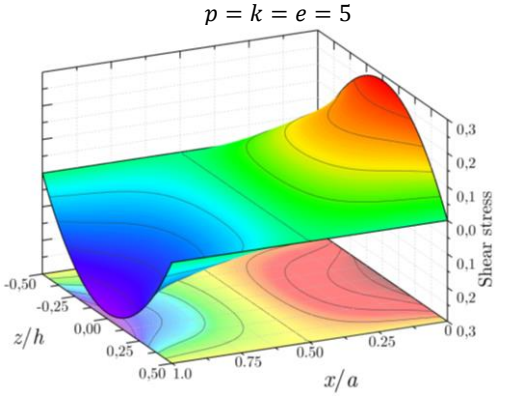

$p = k = e = 10$

Fig. 16 Dimensionless axial stresses $\bar{\sigma}_{xx}$ of softcore coated spherical FG-A GRC shell $(SSSS, W_{GPL} = 5\%)$

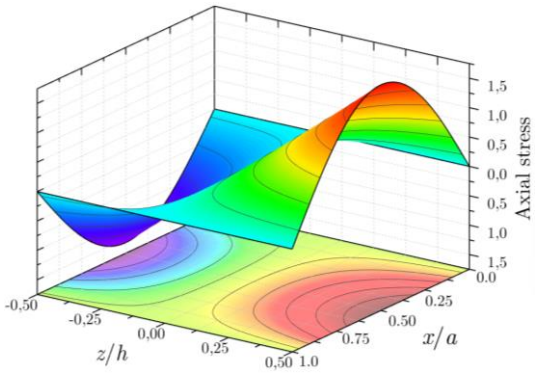

$p = k = e = 0$

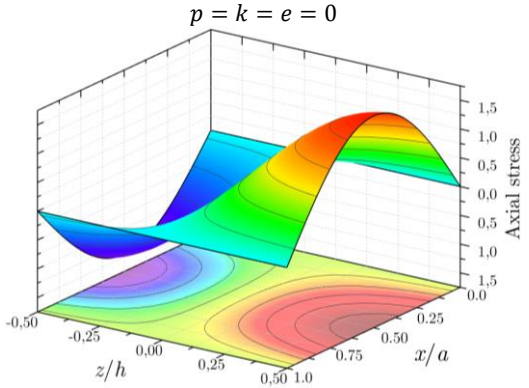

$p = k = e = 2$

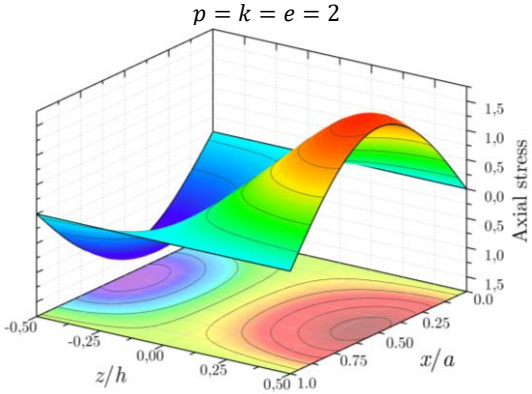

$p = k = e = 5$

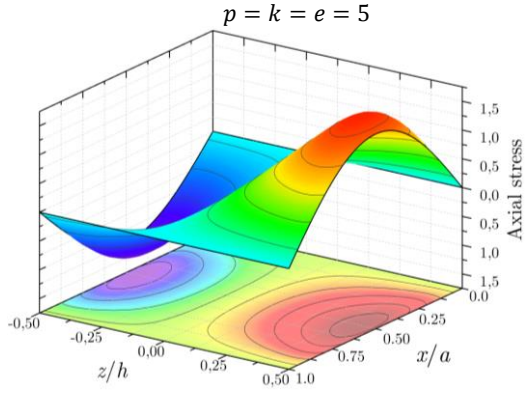

$p = k = e = 10$

Fig. 17 Dimensionless shear stresses $\bar{\tau}_{xz}$ of hardcore coated spherical FG-A GRC shell $(SSSS, W_{GPL} = 5\%)$

of curvature R_x/a is plotted in Fig. 12. Except for the case of aspect ratio $b/a = 0.5$, it is seen that the increase of R_y/b leads to a continue increasing in central deflections.

Dimensionless central deflection of spherical FG GRC shells versus the length-to-width ratio of GPL nanofillers is depicted in Fig. 13 for various GPLs reinforcement. The rise in the thickness-to-length ratio $a_{\mathrm{GPL}}/h_{\mathrm{GPL}}$ leads to a decrement in the deflections of both hardcore and softcore shells.

The same influence is observed in Fig. 14 by varying the

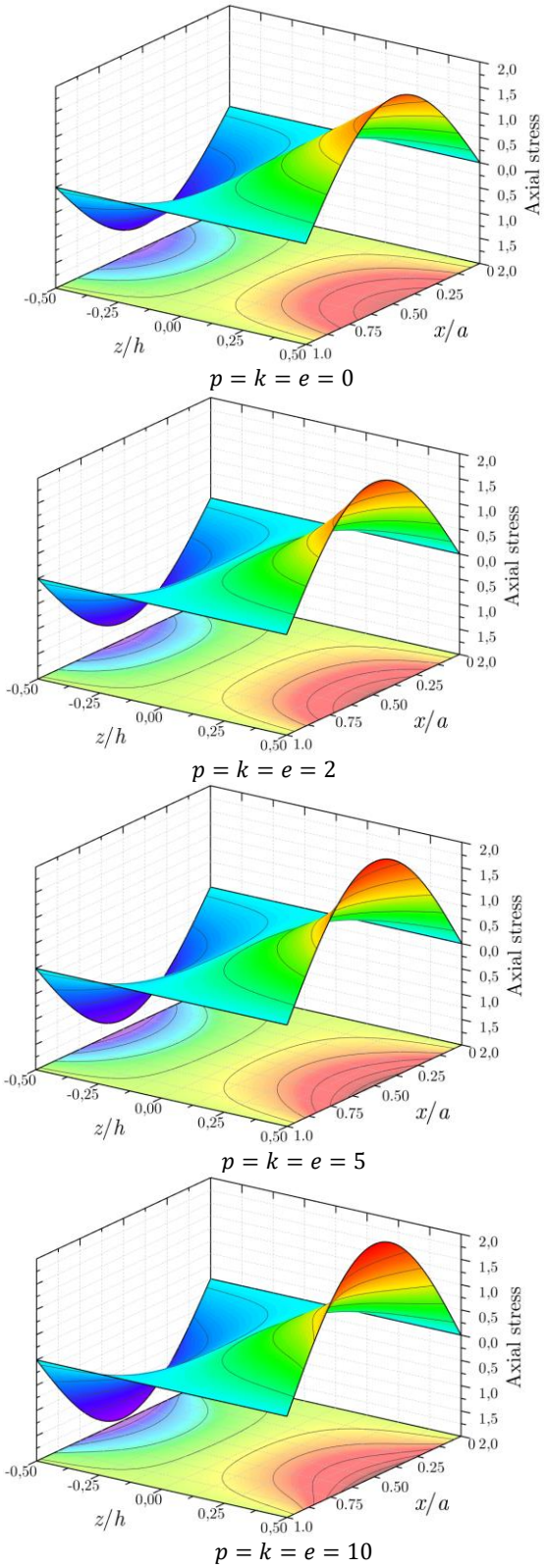

Fig. 18 Dimensionless shear stresses $\bar{\tau}_{xz}$ of softcore coated spherical FG-A GRC shell $(SSSS, W_{GPL} = 5\%)$.

width-to-length ratio $b_{\mathrm{GPL}}/a_{\mathrm{GPL}}$ of the GPLs nano-fillers where the raise in the width-to-length ratio reduces the shell deflection. Fig. 15 shows the action of the inhomogeneity indexes p, k and e on the dimensionless axial stresses $\bar{\sigma}_{xx}$ of hardcore FG-A GRC shell. For the case of homogenous shell $(p = k = e = 0)$, The maximum stresses are accrued at the top and bottom surfaces, which are tensile at the top surface and compressive at the bottom surface. For the other shells, the maximum values of stresses are changed from the top and bottom surfaces to the inside of the shell. On the other hand, in Fig. 16, The maximum stresses are accrued at the top and bottom surfaces regardless of the inhomogeneity parameters. Dimensionless shear stresses $\bar{\tau}_{xz}$ of hardcore coated spherical hardcore and softcore FG-A GRC shell is plotted in Figs. 17 and 18 respectively. For all softcore shells cases in addition to the homogenous shells $(p = k = e = 0)$, the maximum values of the shear stress occur at a point on the mid-plane of the shell, while it is changed to the inside of the shell for the hardcore shells.

7. Conclusions

The static behavior of novel coated functionally graded graphene-reinforced composite shell is examined in this paper. The formulation is exploited to evaluate the bending response and critical buckling loads for these structures. The equation of equilibrium is derived and then solved analytically using Galerkin method. The effective Young's modulus of the GRC shell was estimated using the Halpin-Tsai model, and Poisson's ratio and mass density are obtained by using the rule of mixture. Two types of FG GRC shells, hardcore and softcore, are analyzed, and five different GPLs distribution patterns are considered in this study. Detailed analysis of the effect of the material and geometrical characteristics is carried out. The parametric studies illustrate that:

• The hardcore FG-A GRC shell has the better response among various shell patterns, due to their higher stiffness.

• Increasing the weight fraction enhances the stiffness of the FG-GRC shells.

• Raising length-to-width and length-to-thickness ratios leads to improving the total stiffness of the GRC shell and subsequently leads to lowering the transverse displacements and increasing critical buckling loads.

Acknowledgment

This research was funded by the Institutional Fund Projects under grant no. (IFPIP: 679-135-1443). The authors gratefully acknowledge technical and financial support provided by the Ministry of Education and King Abdulaziz University, DSR in Jeddah, Saudi Arabia.

References

Abazid, M.A., Zenkour, A.M. and Sobhy, M. (2020), "Wave propagation in FG porous GPLs-reinforced nanoplates under in-plane mechanical load and Lorentz magnetic force via a new quasi 3D plate theory", *Mech. Based Des. Struct.*, 1-20. https://doi.org/10.1080/15397734.2020.1769651

Abdelhaffez, G.S., Daikh, A.A., Saleem, H.A. and Eltaher, M.A.

(2023), "Buckling of coated functionally graded spherical nanoshells rested on orthotropic elastic medium", *Mathematics*, **11**(2), 409. https://doi.org/10.3390/math11020409

Abdelrahman, A.A., Esen, I. and Eltaher, M.A. (2021a), "Vibration response of Timoshenko perforated microbeams under accelerating load and thermal environment", *Appl. Math. Comput.*, **407**, 126307. https://doi.org/10.1016/j.amc.2021.126307

Abdelrahman, A.A., Esen, I., Özarpa, C. and Eltaher, M.A. (2021b), "Dynamics of perforated nanobeams subject to moving mass using the nonlocal strain gradient theory", *Appl. Math. Modell.*, **96**, 215-235. https://doi.org/10.1016/j.apm.2021.03.008

Affdl, J.H. and Kardos, J.L. (1976), "The Halpin-Tsai equations: A review", *Polym. Eng. Sci.*, **16**(5), 344-352. https://doi.org/10.1002/pen.760160512

Al-Zahrani, M.A., Asiri, S.A., Ahmed, K.I. and Eltaher, M.A. (2022), "Free vibration analysis of 2D functionally graded strip beam using finite element method", *J. Appl. Comput. Mech.*, **8**(4), 1422-1430.

Assie, A.E., Mohamed, S.M., Shanab, R.A., Abo-bakr, R.M. and Eltaher, M.A. (2023), "Static buckling of 2D fg porous plates resting on elastic foundation based on unified shear theories", *J. Appl. Comput. Mech.*, **9**(1), 239-258.

Bensaid, I., Daikh, A.A. (2020), "Size-dependent free vibration and buckling analysis of sigmoid and power law functionally graded sandwich nanobeams with microstructural defects", *Proceedings of the Institution of Mechanical Engineers, Part C: Journal of Mechanical Engineering Science*, **234**(18), 3667-3688. https://doi.org/10.1177/0954406220916481

Bouadi, A., Bousahla, A.A., Houari, M.S.A., Heireche, H. and Tounsi, A. (2018), "A new nonlocal HSDT for analysis of stability of single layer graphene sheet", *Adv. Nano Res.*, **6**(2), 147-162. http://dx.doi.org/10.12989/anr.2018.6.2.147

Dai, G. and Mishnaevsky Jr, L. (2014), "Graphene reinforced nanocomposites: 3D simulation of damage and fracture", *Comput. Mater. Sci.*, **95**, 684-692. http://doi.org/10.1016/j.commatsci.2014.08.011

Daikh, A.A. and Megueni, A. (2018), "Thermal buckling analysis of functionally graded sandwich plates", *J. Therm. Stress.*, **41**(2), 139-159. https://doi.org/10.1080/01495739.2017.1393644

Daikh, A.A. and Zenkour, A.M. (2020e), "Bending of functionally graded sandwich nanoplates resting on pasternak foundation under different boundary conditions", *J. Appl. Comput. Mech.*, **6**, 1245-1259. https://doi.org/10.22055/JACM.2020.33136.2166

Daikh, A.A., Bachiri, A., Houari, M.S.A. and Tounsi, A. (2020b), "Size dependent free vibration and buckling of multilayered carbon nanotubes reinforced composite nanoplates in thermal environment", *Mech. Based Des. Struct.*, 1-29. https://doi.org/10.1080/15397734.2020.1752232

Daikh, A.A., Bensaid, I. and Zenkour, A.M. (2020d), "Temperature dependent thermomechanical bending response of functionally graded sandwich plates", *Eng. Res. Exp.*, **2**(1), 015006. https://doi.org/10.1088/2631-8695/ab638c

Daikh, A.A., Drai, A., Bensaid, I., Houari, M.S.A. and Tounsi, A. (2020a), "On vibration of functionally graded sandwich nanoplates in the thermal environment", *J. Sandw. Struct. Mater.*, 1099636220909790. https://doi.org/10.1177/1099636220909790

Daikh, A.A., Drai, A., Houari, M.S.A. and Eltaher, M.A. (2020c), "Static analysis of multilayer nonlocal strain gradient nanobeam reinforced by carbon nanotubes", *Steel Compos. Struct.*, **36**(6), 643-656. https://doi.org/10.12989/scs.2020.36.6.643

Daikh, A.A., Houari, M.S.A. and Tounsi, A. (2019), "Buckling analysis of porous FGM sandwich nanoplates due to heat conduction via nonlocal strain gradient theory", *Eng. Res. Exp.*, **1**(1), 015022. https://doi.org/10.1088/2631-8695/ab38f9

Ebrahimi, F., Nouraei, M., Dabbagh, A. and Rabczuk, T. (2020), "Thermal buckling analysis of embedded graphene-oxide powder-reinforced nanocomposite plates", *Adv. Nano Res.*, **7**(4), 293-310. http://dx.doi.org/10.12989/anr.2019.7.5.293

Eltaher, M.A., Agwa, M. and Kabeel, A. (2018), "Vibration analysis of material size-dependent CNTs using energy equivalent model", *J. Appl. Comput. Mech.*, **4**(2), 75-86.

Esen, I., Abdelrhmaan, A.A. and Eltaher, M.A. (2021a), "Free vibration and buckling stability of FG nanobeams exposed to magnetic and thermal fields", *Eng. Comput.*, 1-20. https://doi.org/10.1007/s00366-021-01389-5

Esen, I., Özarpa, C. and Eltaher, M.A. (2021b), "Free vibration of a cracked FG microbeam embedded in an elastic matrix and exposed to magnetic field in a thermal environment", *Compos. Struct.*, **261**, 113552. https://doi.org/10.1016/j.compstruct.2021.113552

Esmaeilzadeh, M., Golmakani, M.A., Kadkhodayan, M., Amoozgar, M. and Bodaghi, M. (2021), "Geometrically nonlinear thermo-mechanical analysis of graphene-reinforced moving polymer nanoplates", *Adv. Nano Res.*, **10**(2), 151-163. http://doi.org/10.12989/anr.2021.10.2.151

Eyvazian, A., Shahsavari, D. and Karami, B. (2020), "On the dynamic of graphene reinforced nanocomposite cylindrical shells subjected to a moving harmonic load", *Int. J. Eng. Sci.*, **154**, 103339. https://doi.org/10.1016/j.ijengsci.2020.103339

Feng, C., Kitipornchai, S. and Yang, J. (2017), "Nonlinear bending of polymer nanocomposite beams reinforced with non-uniformly distributed graphene platelets (GPLs)", *Compos. Part B Eng.*, **110**, 132-140. http://doi.org/10.1016/j.compositesb.2016.11.024

Ghannadpour, S.A.M. and Moradi, F. (2020), "Nonlocal nonlinear analysis of nano-graphene sheets under compression using semi-Galerkin technique", *Adv. Nano Res.*, **7**(5), 311-324. http://doi.org/10.12989/anr.2019.7.5.311

Gholami, R. and Ansari, R. (2019), "Nonlinear stability and vibration of pre/post-buckled multilayer FG-GPLRPC rectangular plates", *Appl. Math. Modell.*, **65**, 627-660. https://doi.org/10.1016/j.apm.2018.08.038

Hadad, M., Babazade, A. and Safarabadi, M. (2020), "Investigation and comparison of the effect of graphene nanoplates and carbon nanotubes on the improvement of mechanical properties in the stir casting process of aluminum matrix nanocomposites", *Int. J. Adv. Manuf. Technol.*, **109**(9), 2535-2547. https://doi.org/10.1007/s00170-020-05838-1

Karami, B., Shahsavari, D., Janghorban, M. and Tounsi, A. (2019), "Resonance behavior of functionally graded polymer composite nanoplates reinforced with graphene nanoplatelets", *Int. J. Mech. Sci.*, **156**, 94-105. https://doi.org/10.1016/j.ijmecsci.2019.03.036

Koochi, A. and Goharimanesh, M. (2021), "Nonlinear oscillations of CNT nano-resonator based on nonlocal elasticity: The energy balance method", *Reports Mech. Eng.*, **2**(1), 41-50. https://doi.org/10.31181/rme200102041g

Lu, L., She, G.L. and Guo, X. (2021a), "Size-dependent postbuckling analysis of graphene reinforced composite micro-tubes with geometrical imperfection", *Int. J. Mech. Sci.*, **199**, 106428. https://doi.org/10.1016/j.ijmecsci.2021.106428

Lu, L., Wang, S., Li, M. and Guo, X. (2021b), "Free vibration and dynamic stability of functionally graded composite microtubes reinforced with graphene platelets", *Compos. Struct.*, **272**, 114231. https://doi.org/10.1016/j.compstruct.2021.114231

Mehrez, S., Karati, S.A., DolatAbadi, P.T., Shah, S.N.R., Azam, S., Khorami, M. and Assilzadeh, H. (2020), "Nonlocal dynamic modeling of mass sensors consisting of graphene sheets based on strain gradient theory", *Adv. Nano Res.*, **9**(4), 221-235. http://doi.org/10.12989/anr.2020.9.4.221

Melaibari, A., Daikh, A.A., Basha, M., Abdalla, A.W., Othman, R., Almitani, K.H., Hamed, M.A. Abdelrahman, A. and Eltaher, M.A. (2022), "Free Vibration of FG-CNTRCs nano-plates/ shells with temperature-dependent properties", *Mathematics*, **10**(4), 583. https://doi.org/10.3390/math10040583

Mohamed, S., Assie, A.E., Mohamed, N. and Eltaher, M.A. (2022), "Static and stress analyses of bi-directional FG porous plate using unified higher order kinematics theories", *Steel Compos. Struct.*, **45**(3), 305-330.

Moradi-Dastjerdi, R., Behdinan, K., Safaei, B. and Qin, Z. (2020), "Static performance of agglomerated CNT-reinforced porous plates bonded with piezoceramic faces", *Int. J. Mech. Sci.*, **188**, 105966. https://doi.org/10.1016/j.ijmecsci.2020.105966

Neves, A.M.A., Ferreira, A.J., Carrera, E., Cinefra, M., Jorge, R. M.N. and Soares, C.M.M. (2012), "Static analysis of functionally graded sandwich plates according to a hyperbolic theory considering Zig-Zag and warping effects", *Adv. Eng. Softw.*, **52**, 30-43. https://doi.org/10.1016/j.advengsoft.2012.05.005

Qin, B., Wang, Q., Zhong, R., Zhao, X. and Shuai, C. (2020), "A three-dimensional solution for free vibration of FGP-GPLRC cylindrical shells resting on elastic foundations: A comparative and parametric study", *Int. J. Mech. Sci.*, **187**, 105896. https://doi.org/10.1016/j.ijmecsci.2020.105896

Ouakad, H.M., Valipour, A., Żur, K.K., Sedighi, H.M. and Reddy, J.N. (2020), "On the nonlinear vibration and static deflection problems of actuated hybrid nanotubes based on the stress-driven nonlocal integral elasticity", *Mech. Mater.*, **148**, 103532. https://doi.org/10.1016/j.mechmat.2020.103532

Rysaeva, L.K., Korznikova, E.A., Murzaev, R.T., Abdullina, D.U., Kudreyko, A.A., Baimova, J.A., Lisovenko, D.S. and Dmitriev, S.V. (2020a), "Elastic damper based on the carbon nanotube bundle", *Facta Univ. Series Mech. Eng.*, **18**(1), 001-012. https://doi.org/10.22190/FUME200128011R

Rysaeva, L.K., Bachurin, D.V., Murzaev, R.T., Abdullina, D.U., Korznikova, E.A., Mulyukov, R.R. and Dmitriev, S.V. (2020b), "Evolution of the carbon nanotube bundle structure under biaxial and shear strains", *Facta Univ. Series Mech. Eng.*, **18**(4), 525-536. https://doi.org/10.22190/FUME201005043R

Safaei, B., Khoda, F.H. and Fattahi, A.M. (2019), "Non-classical plate model for single-layered graphene sheet for axial buckling", *Adv. Nano Res.*, **7**(4), 265-275. http://doi.org/10.12989/anr.2019.7.4.265

Sedighi, H. M. (2014), "Size-dependent dynamic pull-in instability of vibrating electrically actuated microbeams based on the strain gradient elasticity theory", *Acta Astronautica*, **95**, 111-123. https://doi.org/10.1016/j.actaastro.2013.10.020

Sedighi, H.M. and Daneshmand, F. (2014), "Static and dynamic pull-in instability of multi-walled carbon nanotube probes by He's iteration perturbation method", *J. Mech. Sci. Technol.*, **28**, 3459-3469. https://doi.org/10.1007/s12206-014-0807-x

Sedighi, H.M., Ouakad, H.M., Dimitri, R. and Tornabene, F. (2020), "Stress-driven nonlocal elasticity for the instability analysis of fluid-conveying C-BN hybrid-nanotube in a magneto-thermal environment", *Physica Scripta*, **95**(6), 065204. https://doi.org/10.1088/1402-4896/ab793f

Shariati, A., Jung, D.W., Mohammad-Sedighi, H., Żur, K.K., Habibi, M. and Safa, M. (2020), "Stability and dynamics of viscoelastic moving rayleigh beams with an asymmetrical distribution of material parameters", *Symmetry*, 12(4), 586. https://doi.org/10.3390/sym12040586

She, G.L., Liu, H.B. and Karami, B. (2021), "Resonance analysis of composite curved microbeams reinforced with graphene nanoplatelets", *Thin Wall. Struct.*, **160**, 107407. https://doi.org/10.1016/j.tws.2020.107407

She, G.L., Yan, K.M., Zhang, Y.L., Liu, H.B. and Ren, Y.R. (2018), "Wave propagation of functionally graded porous nanobeams based on non-local strain gradient theory", *Eur. Phys. J. Plus*, **133**(9), 1-9. https://doi.org/10.1140/epjp/i2018-12196-5

Shen, H. S., Xiang, Y. and Lin, F. (2017), "Thermal buckling and postbuckling of functionally graded graphene-reinforced composite laminated plates resting on elastic foundations", *Thin Wall. Struct.*, **118**, 229-237. http://doi.org/10.1016/j.tws.2017.05.006

Stankovich, S., Dikin, D.A., Dommett, G.H., Kohlhaas, K.M., Zimney, E.J., Stach, E.A., Piner, R.D., Nguyen, S.T. and Ruoff, R.S. (2006), "Graphene-based composite materials", *Nature*, **442**(7100), 282-286. https://doi.org/10.1038/nature04969

Thai, C.H., Ferreira, A.J.M., Tran, T.D. and Phung-Van, P. (2019), "Free vibration, buckling and bending analyses of multilayer functionally graded graphene nanoplatelets reinforced composite plates using the NURBS formulation", *Compos. Struct.*, **220**, 749-759. https://doi.org/10.1016/j.compstruct.2019.03.100

Uzun, B., Civalek, O. and Aydogdu, I. (2019), "Optimum design of nano-scaled beam using the social spider optimization (SSO) algorithm", *J. Appl. Comput. Mech.*,

Wu, H., Kitipornchai, S. and Yang, J. (2017), "Thermal buckling and postbuckling of functionally graded graphene nanocomposite plates", *Mater. Des.*, **132**, 430-441. https://doi.org/10.1016/j.matdes.2017.07.025

Yang, J., Wu, H. and Kitipornchai, S. (2017), "Buckling and postbuckling of functionally graded multilayer graphene platelet-reinforced composite beams", *Compos. Struct.*, **161**, 111-118. https://doi.org/10.1016/j.compstruct.2016.11.048

Zenkour, A.M. (2013), "Bending analysis of functionally graded sandwich plates using a simple four-unknown shear and normal deformations theory", *J. Sandw. Struct. Mater.*, **15**(6), 629-656. https://doi.org/10.1177/1099636213498886

Zghal, S., Trabelsi, S., Frikha, A. and Dammak, F. (2021), "Thermal free vibration analysis of functionally graded plates and panels with an improved finite shell element", *J. Therm. Stress.*, **44**(3), 315-341. https://doi.org/10.1080/01495739.2021.1871577

Zhang, Y.W., Ding, H.X. and She, G.L. (2022), "Snap-buckling and resonance of functionally graded graphene reinforced composites curved beams resting on elastic foundations in thermal environment", *J. Therm. Stress.*, **45**(12), 1029-1042. https://doi.org/10.1080/01495739.2022.2125137

Zhao, J. L., Chen, X., She, G.L., Jing, Y., Bai, R.Q., Yi, J., Pu, H.Y. and Luo, J. (2022), "Vibration characteristics of functionally graded carbon nanotube-reinforced composite double-beams in thermal environments", *Steel Compos. Struct*, **43**(6), 797-808. https://doi.org/10.12989/scs.2022.43.6.797

Zhao, S., Zhao, Z., Yang, Z., Ke, L., Kitipornchai, S. and Yang, J. (2020), "Functionally graded graphene reinforced composite structures: A review", *Eng. Struct.*, **210**, 110339. https://doi.org/10.1016/j.engstruct.2020.110339

CC

Appendix

Rigidity matrix elements:

$$K_{11} = A_{11}\int_0^a\int_0^b \frac{\partial^3 X_m}{\partial x^3} Y_n \frac{\partial X_m}{\partial x} Y_n \,\mathrm{d}x\mathrm{d}y + A_{66}\int_0^a\int_0^b \frac{\partial X_m}{\partial x}\frac{\partial^2 Y_n}{\partial y^2}\frac{\partial X_m}{\partial x} Y_n \,\mathrm{d}x\mathrm{d}y$$

$$K_{12} = (A_{12} + A_{66})\int_0^a\int_0^b \frac{\partial X_m}{\partial x}\frac{\partial^2 Y_n}{\partial y^2}\frac{\partial X_m}{\partial x} Y_n \,\mathrm{d}x\mathrm{d}y$$

$$K_{13} = \left(\frac{A_{11}}{R_x} + \frac{A_{12}}{R_y}\right)\int_0^a\int_0^b \frac{\partial X_m}{\partial x} Y_n \frac{\partial X_m}{\partial x} Y_n \,\mathrm{d}x\mathrm{d}y - B_{11}\int_0^a\int_0^b \frac{\partial^3 X_m}{\partial x^3} Y_n \frac{\partial X_m}{\partial x} Y_n \,\mathrm{d}x\mathrm{d}y - (B_{12} + 2B_{66})\int_0^a\int_0^b \frac{\partial X_m}{\partial x}\frac{\partial^2 Y_n}{\partial y^2}\frac{\partial X_m}{\partial x} Y_n \,\mathrm{d}x\mathrm{d}y$$

$$K_{14} = B_{11}^s\int_0^a\int_0^b \frac{\partial^3 X_m}{\partial x^3} Y_n \frac{\partial X_m}{\partial x} Y_n \,\mathrm{d}x\mathrm{d}y + B_{66}^s\int_0^a\int_0^b \frac{\partial X_m}{\partial x}\frac{\partial^2 Y_n}{\partial y^2}\frac{\partial X_m}{\partial x} Y_n \,\mathrm{d}x\mathrm{d}y$$

$$K_{15} = (B_{12}^s + B_{66}^s)\int_0^a\int_0^b \frac{\partial X_m}{\partial x}\frac{\partial^2 Y_n}{\partial y^2}\frac{\partial X_m}{\partial x} Y_n \,\mathrm{d}x\mathrm{d}y$$

$$K_{21} = (A_{12} + A_{66})\int_0^a\int_0^b \frac{\partial^2 X_m}{\partial x^1}\frac{\partial Y_n}{\partial y} X_m \frac{\partial Y_n}{\partial y}\mathrm{d}x\mathrm{d}y$$

$$K_{22} = A_{22}\int_0^a\int_0^b X_m \frac{\partial^3 Y_n}{\partial y^3} X_m \frac{\partial Y_n}{\partial y}\mathrm{d}x\mathrm{d}y + A_{66}\int_0^a\int_0^b\int_0^b \frac{\partial^2 X_m}{\partial x^2}\frac{\partial Y_n}{\partial y} X_m \frac{\partial Y_n}{\partial y}\mathrm{d}x\mathrm{d}y$$

$$K_{23} = \left(\frac{A_{12}}{R_x} + \frac{A_{22}}{R_y}\right)\int_0^a\int_0^b X_m \frac{\partial Y_n}{\partial y} X_m \frac{\partial Y_n}{\partial y}\mathrm{d}x\mathrm{d}y - B_{22}\int_0^a\int_0^b X_m \frac{\partial^3 Y_n}{\partial y^3} X_m \frac{\partial Y_n}{\partial y}\mathrm{d}x\mathrm{d}y - (B_{12} + 2B_{66})\int_0^a\int_0^b \frac{\partial^2 X_m}{\partial x^2}\frac{\partial Y_n}{\partial y} X_m \frac{\partial Y_n}{\partial y}\mathrm{d}x\mathrm{d}y$$

$$K_{24} = (B_{12}^s + B_{66}^s)\int_0^a\int_0^b \frac{\partial^2 X_m}{\partial x^2}\frac{\partial Y_n}{\partial y} X_m \frac{\partial Y_n}{\partial y}\mathrm{d}x\mathrm{d}y$$

$$K_{25} = B_{22}^s\int_0^a\int_0^b X_m \frac{\partial^3 Y_n}{\partial y^3} X_m \frac{\partial Y_n}{\partial y}\mathrm{d}x\mathrm{d}y + B_{66}^s\int_0^a\int_0^b \frac{\partial^2 X_m}{\partial x^2}\frac{\partial Y_n}{\partial y} X_m \frac{\partial Y_n}{\partial y}\mathrm{d}x\mathrm{d}y$$

$$K_{31} = -\left(\frac{A_{11}}{R_x} + \frac{A_{12}}{R_y}\right)\int_0^a\int_0^b \frac{\partial^2 X_n}{\partial x^2} Y_n X_m Y_n \,\mathrm{d}x\mathrm{d}y + B_{11}\int_0^a\int_0^b \frac{\partial^4 X_n}{\partial x^4} Y_n X_m Y_n \,\mathrm{d}x\mathrm{d}y + (B_{12} + 2B_{66})\int_0^a\int_0^b \frac{\partial^2 X_m}{\partial x^2}\frac{\partial^2 Y_n}{\partial y^2} X_m Y_n \,\mathrm{d}x\mathrm{d}y$$

$$K_{32} = -\left(\frac{A_{12}}{R_x} + \frac{A_{22}}{R_y}\right)\int_0^a\int_0^b X_m \frac{\partial^2 Y_n}{\partial y^2} X_m Y_n \,\mathrm{d}x\mathrm{d}y + B_{22}\int_0^a\int_0^b X_m \frac{\partial^4 Y_n}{\partial y^4} X_m Y_n \,\mathrm{d}x\mathrm{d}y + (B_{12} + 2B_{66})\int_0^a\int_0^b \frac{\partial^2 X_m}{\partial x^2}\frac{\partial^2 Y_n}{\partial y^2} X_m Y_n \,\mathrm{d}x\mathrm{d}y$$

$$K_{33} = 2\left(\frac{B_{11}}{R_x} + \frac{B_{12}}{R_y}\right)\int_0^a\int_0^b \frac{\partial^2 X_n}{\partial x^2} Y_n X_m Y_n \,\mathrm{d}x\mathrm{d}y + 2\left(\frac{B_{12}}{R_x} + \frac{B_{22}}{R_y}\right)\int_0^a\int_0^b X_m \frac{\partial^2 Y_n}{\partial y^2} X_m Y_n \,\mathrm{d}x\mathrm{d}y - \left(\frac{A_{11}}{{R_x}^2} + 2\frac{A_{12}}{R_x R_y} + \frac{A_{22}}{{R_y}^2}\right)\int_0^a\int_0^b X_m Y_n X_m Y_n \,\mathrm{d}x\mathrm{d}y - D_{11}\int_0^a\int_0^b \frac{\partial^4 X_m}{\partial x^4} Y_n X_m Y_n \,\mathrm{d}x\mathrm{d}y - D_{22}\int_0^a\int_0^b X_m \frac{\partial^4 Y_n}{\partial y^4} X_m Y_n \,\mathrm{d}x\mathrm{d}y - 2(D_{12} + 2D_{66})\int_0^a\int_0^b \frac{\partial^2 X_m}{\partial x^2}\frac{\partial^2 Y_n}{\partial y^2} X_m Y_n \,\mathrm{d}x\mathrm{d}y + \bar{N}_{xx}^0\int_0^a\int_0^b \frac{\partial^2 X_m}{\partial x^2} Y_n X_m Y_n \,\mathrm{d}x\mathrm{d}y + + \bar{N}_{yy}^0\int_0^a\int_0^b X_m \frac{\partial^2 Y_n}{\partial y^2} X_m Y_n \,\mathrm{d}x\mathrm{d}y$$

$$K_{34} = -\left(\frac{B_{11}^s}{R_x} + \frac{B_{12}^s}{R_y}\right)\int_0^a\int_0^b \frac{\partial^2 X_n}{\partial x^2} Y_n X_m Y_n \,\mathrm{d}x\mathrm{d}y + D_{11}^s\int_0^a\int_0^b \frac{\partial^4 X_m}{\partial x^4} Y_n X_m Y_n \,\mathrm{d}x\mathrm{d}y + (D_{12}^s + 2D_{66}^s)\int_0^a\int_0^b \frac{\partial^2 X_m}{\partial x^2}\frac{\partial^2 Y_n}{\partial y^2} X_m Y_n \,\mathrm{d}x\mathrm{d}y$$

$$K_{35} = -\left(\frac{B_{12}^s}{R_x} + \frac{B_{22}^s}{R_y}\right)\int_0^a\int_0^b X_m \frac{\partial^2 Y_n}{\partial y^2} X_m Y_n \,\mathrm{d}x\mathrm{d}y + D_{22}^s\int_0^a\int_0^b X_m \frac{\partial^4 Y_n}{\partial y^4} X_m Y_n \,\mathrm{d}x\mathrm{d}y + (D_{12}^s + 2D_{66}^s)\int_0^a\int_0^b \frac{\partial^2 X_m}{\partial x^2}\frac{\partial^2 Y_n}{\partial y^2} X_m Y_n \,\mathrm{d}x\mathrm{d}y$$

$$K_{41} = B_{11}^s\int_0^a\int_0^b \frac{\partial^3 X_m}{\partial x^3} Y_n \frac{\partial X_m}{\partial x} Y_n \,\mathrm{d}x\mathrm{d}y + B_{66}^s\int_0^a\int_0^b \frac{\partial X_m}{\partial x}\frac{\partial^2 Y_n}{\partial y^2}\frac{\partial X_m}{\partial x} Y_n \,\mathrm{d}x\mathrm{d}y$$

$$K_{42} = (B_{12}^s + B_{66}^s)\int_0^a\int_0^b \frac{\partial X_m}{\partial x}\frac{\partial^2 Y_n}{\partial y^2}\frac{\partial X_m}{\partial x} Y_n \,\mathrm{d}x\mathrm{d}y$$

$$K_{43} = \left(\frac{B_{11}^s}{R_x} + \frac{B_{12}^s}{R_y}\right)\int_0^a\int_0^b \frac{\partial X_m}{\partial x} Y_n \frac{\partial X_m}{\partial x} Y_n \,\mathrm{d}x\mathrm{d}y - D_{11}^s\int_0^a\int_0^b \frac{\partial^3 X_m}{\partial x^3} Y_n \frac{\partial X_m}{\partial x} Y_n \,\mathrm{d}x\mathrm{d}y - (D_{12}^s + 2D_{66}^s)\int_0^a\int_0^b \frac{\partial X_m}{\partial x}\frac{\partial^2 Y_n}{\partial y^2}\frac{\partial X_m}{\partial x} Y_n \,\mathrm{d}x\mathrm{d}y$$

$$K_{44} = F_{11}^s\int_0^a\int_0^b \frac{\partial^3 X_m}{\partial x^3} Y_n \frac{\partial X_m}{\partial x} Y_n \,\mathrm{d}x\mathrm{d}y + F_{66}^s\int_0^a\int_0^b \frac{\partial X_m}{\partial x}\frac{\partial^2 Y_n}{\partial y^2}\frac{\partial X_m}{\partial x} Y_n \,\mathrm{d}x\mathrm{d}y - A_{44}^s\int_0^a\int_0^b \frac{\partial X_m}{\partial x} Y_n \frac{\partial X_m}{\partial x} Y_n \,\mathrm{d}x\mathrm{d}y$$

$$K_{45} = (F_{12}^s + F_{66}^s)\int_0^a\int_0^b \frac{\partial X_m}{\partial x}\frac{\partial^2 Y_n}{\partial y^2}\frac{\partial X_m}{\partial x} Y_n \,\mathrm{d}x\mathrm{d}y$$

$$K_{51} = (B_{12}^s + B_{66}^s)\int_0^a\int_0^b \frac{\partial^2 X_m}{\partial x^2}\frac{\partial Y_n}{\partial y} X_m \frac{\partial Y_n}{\partial y}\mathrm{d}x\mathrm{d}y$$

$$K_{52} = B_{22}^s\int_0^a\int_0^b X_m \frac{\partial^3 Y_n}{\partial y^3} X_m \frac{\partial Y_n}{\partial y}\mathrm{d}x\mathrm{d}y + B_{66}^s\int_0^a\int_0^b \frac{\partial^2 X_m}{\partial x^2}\frac{\partial Y_n}{\partial y} X_m \frac{\partial Y_n}{\partial y}\mathrm{d}x\mathrm{d}y$$

$$K_{53} = \left(\frac{B_{12}^s}{R_x} + \frac{B_{22}^s}{R_y}\right)\int_0^a\int_0^b X_m \frac{\partial Y_n}{\partial y} X_m \frac{\partial Y_n}{\partial y}\mathrm{d}x\mathrm{d}y - D_{22}^s\int_0^a\int_0^b X_m \frac{\partial^3 Y_n}{\partial y^3} X_m \frac{\partial Y_n}{\partial y}\mathrm{d}x\mathrm{d}y - (D_{12}^s + 2D_{66}^s)\int_0^a\int_0^b \frac{\partial^2 X_m}{\partial x^2}\frac{\partial Y_n}{\partial y} X_m \frac{\partial Y_n}{\partial y}\mathrm{d}x\mathrm{d}y$$

$$K_{54} = (F_{12}^s + F_{66}^s)\int_0^a\int_0^b \frac{\partial^2 X_m}{\partial x^2}\frac{\partial Y_n}{\partial y} X_m \frac{\partial Y_n}{\partial y}\mathrm{d}x\mathrm{d}y$$

$$K_{55} = F_{22}^s\int_0^a\int_0^b X_m \frac{\partial^3 Y_n}{\partial y^3} X_m \frac{\partial Y_n}{\partial y}\mathrm{d}x\mathrm{d}y + F_{66}^s\int_0^a\int_0^b \frac{\partial^2 X_m}{\partial x^2}\frac{\partial Y_n}{\partial y} X_m \frac{\partial Y_n}{\partial y}\mathrm{d}x\mathrm{d}y - A_{55}^s\int_0^a\int_0^b X_m \frac{\partial Y_n}{\partial y} X_m \frac{\partial Y_n}{\partial y}\mathrm{d}x\mathrm{d}y$$